ELSEVIER

Quaternary Science Reviews 26 (2007) 170–188

QSR

Holocene ITCZ and Indian monsoon dynamics recorded in stalagmites from Oman and Yemen (Socotra)

Dominik Fleitmann[a,*], Stephen J. Burns[b], Augusto Mangini[c], Manfred Mudelsee[d], Jan Kramers[a], Igor Villa[a], Ulrich Neff[c], Abdulkarim A. Al-Subbary[e], Annett Buettner[a], Dorothea Hippler[a], Albert Matter[a]

[a]*Institute of Geological Sciences, University of Bern, Bern, Switzerland*
[b]*Department of Geosciences, Morrill Science Center, University of Massachusetts, Amherst, MA, USA*
[c]*Heidelberg Academy of Sciences, Heidelberg, Germany*
[d]*Meteorological Institute, University of Leipzig, Leipzig, Germany*
[e]*Department of Earth and Environmental Science, Faculty of Science, University of Sana'a, Sana'a, Republic of Yemen*

Received 22 February 2005; accepted 25 April 2006

Abstract

High-resolution oxygen isotope ($\delta^{18}O$) profiles of Holocene stalagmites from four caves in Northern and Southern Oman and Yemen (Socotra) provide detailed information on fluctuations in precipitation along a latitudinal transect from 12°N to 23°N. $\delta^{18}O$ values reflect the amount of precipitation which is primarily controlled by the mean latitudinal position of the ITCZ and dynamics of the Indian summer monsoon (ISM). During the early Holocene rapidly decreasing $\delta^{18}O$ values indicate a rapid northward displacement in the mean latitudinal position of the summer ITCZ and the associated ISM rainfall belt, with decadal- to centennial-scale changes in monsoon precipitation correlating well with high-latitude temperature variations recorded in Greenland ice cores. During the middle to late Holocene the summer ITCZ continuously migrated southward and monsoon precipitation decreased gradually in response to decreasing solar insolation, a trend, which is also recorded in other monsoon records from the Indian and East Asian monsoon domains. Importantly, there is no evidence for an abrupt middle Holocene weakening in monsoon precipitation. Although abrupt monsoon events are apparent in all monsoon records, they are short-lived and clearly superimposed on the long-term trend of decreasing monsoon precipitation. For the late Holocene there is an anti-correlation between ISM precipitation in Oman and inter-monsoon (spring/autumn) precipitation on Socotra, revealing a possible long-term change in the duration of the summer monsoon season since at least 4.5 ka BP. Together with the progressive shortening of the ISM season, gradual southward retreat of the mean summer ITCZ and weakening of the ISM, the total amount of precipitation decreased in those areas located at the northern fringe of the Indian and Asian monsoon domains, but increased in areas closer to the equator.

1. Introduction

The seasonal migration of the Intertropical Convergence Zone (ITCZ)—a narrow latitudinal zone of wind convergence and precipitation—determines the onset, duration and termination of the rainy season in the tropics and subtropics. Variations in the mean latitudinal position and structure of the ITCZ affects tropical and also extra tropical climate on a variety of time scales, ranging from monthly to millennial. For the Holocene, paleoclimate records from many parts of the tropics now reveal that shifts in the mean latitudinal position of ITCZ were accompanied by significant changes in the hydrological cycle (e.g., An et al., 2000; deMenocal, 2000; Gasse, 2000; Maslin and Burns, 2000; Seltzer et al., 2000; Haug et al.,

*Corresponding author. Department of Geosciences, University of Massachusetts, 611 N, Pleasant Street, Amherst, USA.
Tel.: +1 650 725 0927; fax: +1 650 725 2199.
E-mail address: fleitman@geo.umass.edu (D. Fleitmann).

0277-3791/$ - see front matter © 2006 Elsevier Ltd. All rights reserved.
doi:10.1016/j.quascirev.2006.04.012

2001; Fleitmann et al., 2003a; Dykoski et al., 2005; Wang et al., 2005). In order to monitor ITCZ-induced changes in the spatial distribution, seasonality and amount of precipitation, a dense network of well-resolved and continuous paleoclimate records is required. In the Indian summer monsoon (ISM) domain, however, such a network does not yet exist, although there is a relatively large number of marine and continental climate records available from this area (Fig. 1). The majority of these records are based on lacustrine sequences that, along with the marine records, have chronological uncertainties due to so-called "hard water" and "reservoir" effects (e.g., see discussions in Gasse, 2000; Staubwasser et al., 2002) that often make correlation amongst them difficult. In addition to chronological difficulties, low resolution and temporal gaps, as summarized in Fig. 1, represent an additional hindrance. As a result of these shortcomings, considerable discrepancies regarding the mean latitudinal position of the summer ITCZ and the associated belt of maximum precipitation exist. Also, whether Indian and Asian summer monsoon (ASM) precipitation decreased gradually or abruptly during the middle to late Holocene is subject of ongoing debates and two contrasting hypothesis exist: (1) The ISM and ASM weakened abruptly between ~5–4.5 ka BP (Morrill et al., 2003) and (2) more gradually, mimicking decreasing orbitally induced solar insolation (Gupta et al., 2003; Fleitmann et al., 2003a; Dykoski et al., 2005; Ivanochko et al., 2005; Wang et al., 2005).

A further general question is the origin of the ISM and its interaction with the ITCZ. The more traditional view is that the monsoon is driven by land-sea thermal contrast ("gigantic sea-land breeze") between the Eurasian landmass and the Southern Indian Ocean (Webster et al., 1998). However, recent work suggest that the ISM is an integral

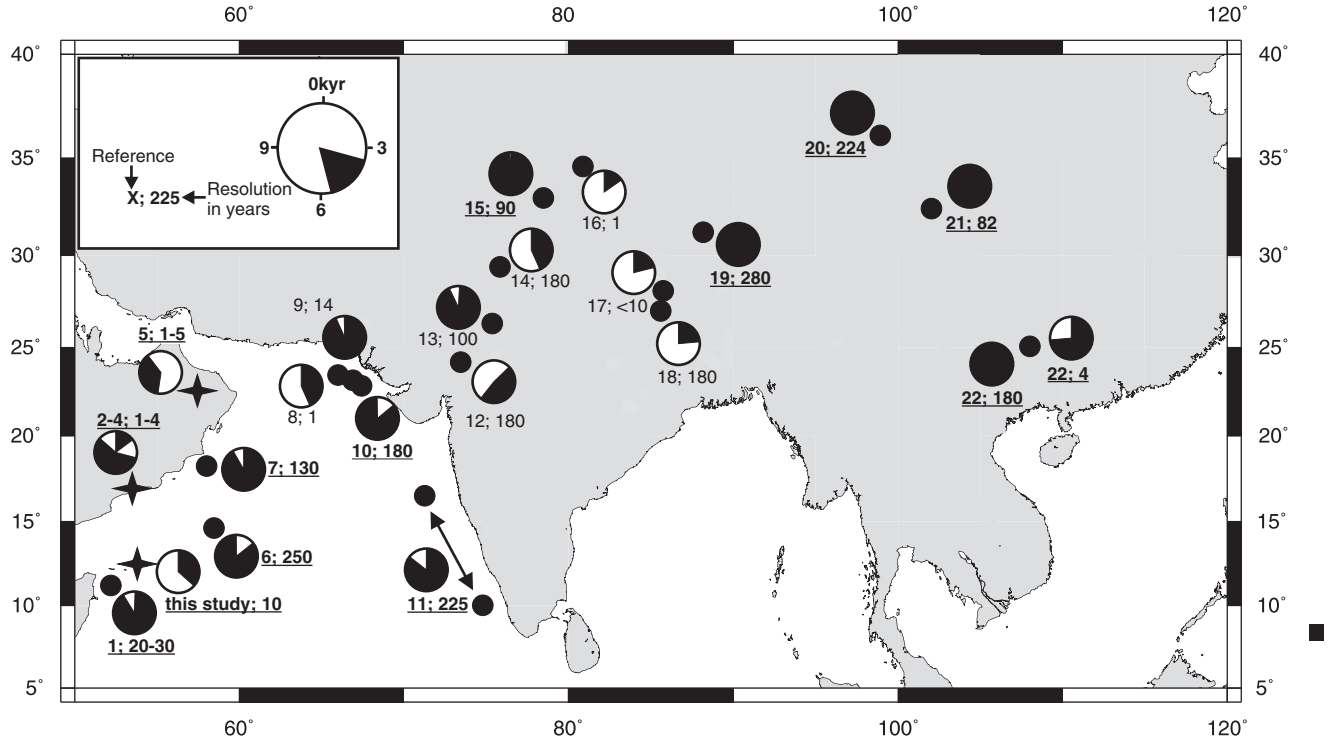

Reference

1	Jung *et al.*, 2002, 2004	12	Prasad *et al.*, 1997
2	Burns *et al.*, 2002	13	Enzel *et al.*, 1999
3	Fleitmann *et al.*, 2003	14	Singh *et al.*, 1974
4	Fleitmann *et al.*, 2004	15	Gasse *et al.*, 1996
5	Neff *et al.*, 2001; this study	16	Thompson *et al.*, 2000
6	Sirocko *et al.*, 1993, 1996	17	Thompson *et al.*, 1995
7	Gupta *et al.*, 2003	18	Denniston *et al.*, 2000
8	von Rad *et al.*, 1999	19	Gu *et al.*, 1993
9	Staubwasser *et al.*, 2002, 2003	20	Lister *et al.*, 1991
10	Schulz *et al.*, 1998	21	Hong *et al.*, 2003
11	Sarkar *et al.*, 2000	22	Dykowski *et al.*, 2005; Wang *et al.*, 2005

Fig. 1. Location map of Holocene continental and marine records from the Indian and Asian monsoon domains, whereas the focus is on continental records. The filled section of the "wheel-diagram" shows the time interval represented by each record. Assigned numbers denote references listed below and temporal resolution for the time series. Underlined bold numbers denote records displayed in Figs. 7 and 8. Star symbols denotes cave sites in Oman and Yemen (Denniston et al., 2000; Gasse et al., 1996; Jung et al., 2004; Prasad et al., 1997; Singh et al., 1974; Thompson et al., 2000).

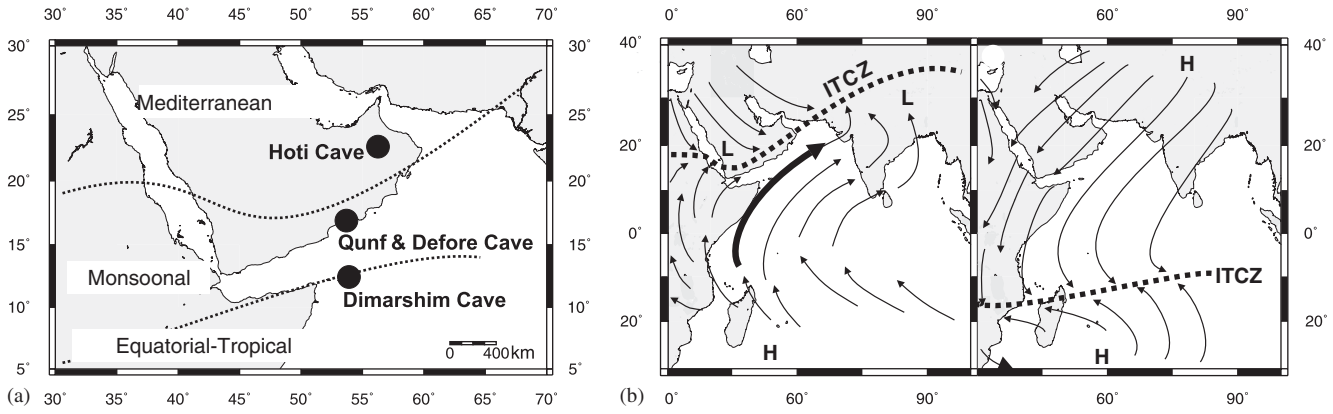

Fig. 2. (a) Precipitation regimes (adapted by Gasse, 2000). "Mediterranean" = winter rainfall, "Monsoonal" = summer monsoon rainfall and "Equatorial-Tropical" = spring and autumn rainfall. Black dots denote location of studied caves. Schematic figures of surface wind pattern during (b) boreal summer (ISM season) and (c) boreal winter (northeast monsoon season). Bold dashed line marks the location of the ITCZ. Bold arrow marks the location of the Findlater Jet also known as Somali Jet.

part of the ITCZ and the manifestation of the seasonal migration of the ITCZ (Chao and Chen, 2001; Gadgil, 2003). Which one of these two explanations describes the dynamics of the ISM better remains unsolved. As mentioned earlier, a dense network of climatic time-series might shed some light on the relationship between the ITCZ and the ISM. One possible source of such records is from stalagmite-based oxygen isotope ($\delta^{18}O$) profiles, as demonstrated by recently published results from Oman (Neff et al., 2001; Burns et al., 2002; Fleitmann et al., 2003a, 2004). However, the isotopic time-series are fragmentary (Fig. 1), such as for Northern Oman where no information currently exists for the period after ~6.3 ka BP. Also, the existing stalagmite records span only a relatively narrow latitudinal transect ranging from 17° to 23°N, which is not sufficient to monitor larger-scale shifts in the mean latitudinal position of the ITCZ during the Holocene.

To aid in filling existing temporal and spatial gaps in climate records, we present two new high-resolution oxygen isotope records, one from Northern Oman (stalagmite H12, Hoti Cave; Fig. 2a) and one from Socotra (stalagmite D1, Dimarshim Cave, Yemen; Fig. 2a). Socotra, located at 12°N in the Northern Indian Ocean, is ideally located to monitor both variations in the mean latitudinal position of the ITCZ and variations in monsoon intensity as it is located within the axis of the Findlater Jet (Fig. 2b; Findlater, 1969). By comparing all stalagmite records, sampled along a ~1200 km long north–south transect that spans three different precipitation regimes (Fig. 2a), we hope to monitor past displacements in the mean latitudinal position of the summer ITCZ and associated changes in the location of the rainfall belt in greater detail. Finally, we compare multiple monsoon records from the ISM and ASM domains to demonstrate that monsoon precipitation decreased gradually since the beginning of the middle Holocene in response to the progressive decrease in summer insolation.

2. Climatic and environmental settings

2.1. Atmospheric circulation in the Indian Ocean

The annual migration of the ITCZ and seasonal development of the monsoon winds are key-components of the climatology in the Indian Ocean and the surrounding areas. In spring the ITCZ migrates northward across the Indian Ocean and reaches its northernmost position during boreal summer (Fig. 2b). From June to September, a strong low-level monsoonal air flow is generated by a strong pressure gradient between the low-pressure cell over the Tibetan Plateau and a high-pressure cell over the Southern Indian Ocean (Fig. 2b). North of the equator, a strong southwesterly air flow, also known as the Somali or Findlater Jet (Findlater, 1969) transports large quantities of moisture, that is then released as monsoon precipitation over some parts of Southern Arabia and the Indian subcontinent. The release of latent heat through condensation of moisture is an additional and important forcing of the ISM as it further strengthens and maintains the surface low pressure over the Asian landmass (Webster et al., 1998). In autumn the ITCZ then retreats southward and reaches its southernmost position at approximately 25°S in January (Fig. 2c). The reversed pressure gradient during the winter months generates the moderate and dry northeast monsoon.

2.2. Climate settings at the cave sites

Stalagmites were collected in four caves located in three areas (Fig. 2a): (1) Northern Oman (Hoti Cave; 23°05′N, 57°21′E; ~800 m above sea level (masl)), (2) Southern Oman (Qunf Cave; 17°10′N, 54°18′E; 650 masl and Defore Cave, 17°07′N, 54°05′E; ~150 masl) and (3) Socotra (Yemen, Dimarshim Cave; 12°33′N, 53.41′E; ~350 masl). As study sites are located along a north–south transect of ~1200 km, seasonal distribution of rainfall differs

significantly (Fig. 2a), being uni-modal in Oman and bi-modal on Socotra. In Northern Oman today, the primary source of rainfall is Mediterranean frontal systems, which are most frequent between January and March (Weyhenmeyer et al., 2002). Additional but minor sources are local convective storm cells which occur during very hot summers and tropical cyclones that reach Northern Oman once every 5–10 years (Weyhenmeyer et al., 2000, 2002). Total annual rainfall in Northern Oman is low and typically ranges from ~55 to 255 mm yr^{-1} in the vicinity of Hoti Cave (station Al Hamra, 700 masl, 1974–97). In contrast to Northern Oman, Southern Oman receives more than 80% of its total annual rainfall, ranging between 200 and 600 mm yr^{-1} (Fleitmann et al., 2004), during the summer monsoon season (regionally known as "Khareef"), which lasts between July and September. Socotra, the southernmost study site, experiences two rainy seasons: one lasting from May to June and one from September to December (Mies and Beyhl, 1996). Both rainy seasons are associated with passages of the ITCZ. Virtually no rainfall occurs during the northeast and southwest monsoon, as the strong divergent surface airflow, particularly during the summer monsoon, suppresses convergence of moisture over the northern Indian Ocean. Total annual rainfall on Socotra varies between approximately 120 and 400 mm yr^{-1} (Mies and Beyhl, 1996).

3. Materials and methods

Six stalagmites, between 30 and 100 cm long, were collected as whole samples or by drilling. All specimens were cut parallel to their growth axis using a diamond saw and then polished. The chronologies are all based on a total of 68 Uranium-series ages (Table 1), which were in part performed on a multi-collector thermal ionization mass spectrometer (TIMS) and in part on a multi-collector inductively coupled plasma mass spectrometer (MC ICP–MS).

For MC ICP–MS analyses, 0.1–0.2 g of sample chip were spiked with a mixed ^{229}Th–^{236}U spike and dissolved in HNO_3 and taken to dryness. Organic material, if present, was attacked with 0.5 ml of $H_2O_2 + HNO_3$(conc). U and Th were separated on anion columns using a 0.5 ml Dowex 1×8 resin bed. A first separation, using 7N HNO_3, produced a pure Th fraction and an impure U fraction, which was purified on the same columns using 6N HCl. After evaporation, the fractions were again treated with $H_2O_2 + HNO_3$(conc) to remove organic remnants from the resin.

U and Th mass spectrometry was done on a Nu Instruments® multicollector ICP–MS equipped with an ESI Apex® desolvating system without membrane and using a self-aspirating nebulizer. With an uptake rate of ca 50 µl/min the ion yield for U and Th was about 70 V/ppm.

U measurements were done from 0.5 N HNO_3 solutions in static mode, whereby masses 236 and 234 were measured in parallel electron multipliers and 235 and 238 in Faraday cups. Baselines were taken on either side of peaks and interpolated. The electron multiplier yield was calibrated every 4 samples by running a NIST U050 solution. The $^{238}U/^{235}U$ ratio was used for instrumental fractionation correction if the ^{238}U signal was greater than 1 V (10^{-11} A); if smaller, the fractionation factor was input from bracketing standards. Normal washout time for U between samples was 5 min with 0.5 N HNO_3 (<1‰ memory); longer washout times were used where significant isotope differences between samples were expected. Runs on the NIST U960 standard yielded $\delta(^{234}U/^{238}U)$ -37.2 ± 2.1‰ (1SD, $N = 35$), where the equilibrium ratio is after Cheng et al. (2000). Th measurements were made from 3 N HCl solutions in a two-cycle multicollector dynamic mode, whereby one electron multiplier, equipped with a WARP filter, alternatingly measured masses 229 and 230. U standard was added to Th run solutions for two reasons, first, to enable correction for instrumental mass fractionation, and second, to provide a reference isotope (238) to eliminate the effects of plasma flicker in obtaining the $^{229}Th/^{230}Th$ ratios. Variations of U and Th signals during the run are fully correlated if no organic matter is present. Baselines were measured at 229.5 and 230.5 for samples and standards with significant ($>10^{-12}$ A) ^{232}Th. For stalagmites the baseline was quite flat and measured at 230.5. Washout time was 15 min to 1‰ of the Th signal, if the capillary and nebulizer were free of organics.

Analytical procedures and details of TIMS measurements are described in detail by Neff et al. (2001) and Fleitmann et al. (2003a). As a result of spike recalibration in 2005 and calibration against the "HU-1" uraninite standard solution (assuming that uraninite is at secular equilibrium for the ^{230}Th–^{234}U–^{238}U sequence), previously published TIMS Th–U dates were by approximately 1% too young. The updated Th–U dates are displayed in Table 1.

A total of 5400 oxygen isotope samples were measured. For each analysis, ~5 mg of powder was drilled from the sample and analyzed with an on-line, automated carbonate system linked to a VG PRISM ratio mass spectrometer. For stalagmite D1 (Dimarshim Cave, Socotra) oxygen isotope ratios were measured on a Delta-plusXL mass spectrometer equipped with an automated carbonate preparation system (Kiel III). All oxygen isotope values are reported in parts per mil (‰) relative to the Vienna PeeDee Belemnite standard (VPDB).

4. Results

4.1. Age calibration

Age-depth plots for all stalagmites are shown in Fig. 3a–f. The chronologies of all stalagmites are based on either interpolation between individual Th–U samples or polynomial fit to the age-depth curve of the Th–U data.

Table 1
Results of Uranium-series dating. Th–U ages measured using MC–ICP–MS are marked with a star (*) symbol

Sample	Depth (mm)	c(Th)		c(U)		(234U/238U)		(230Th/232Th)		(230Th/234U)		Age	
		(ppb)	±	(ppb)	±		±		±		±	(ka)	±
H5	5	198.676	2.204	3362.0	9.3	1.4999	0.0041	5.15	0.16	0.0569	0.0016	6.414	0.188
H5	25	55.876	0.676	9023.2	51.5	1.5133	0.0086	44.53	1.01	0.0586	0.0011	6.582	0.137
H5	65	8.029	0.020	4978.1	7.0	1.6128	0.0036	201.46	1.00	0.0657	0.0003	7.391	0.038
H5	98	10.309	0.075	3950.7	10.0	1.6134	0.0067	136.67	1.70	0.0720	0.0008	8.119	0.092
H5	135	7.034	0.035	4419.8	14.1	1.6003	0.0060	222.71	2.16	0.0723	0.0006	8.153	0.084
H5	160	10.832	0.081	4226.6	10.7	1.5887	0.0063	136.43	1.79	0.0717	0.0008	8.083	0.095
H5	175	21.750	0.318	4074.0	19.7	1.5864	0.0129	71.24	2.15	0.0777	0.0021	8.788	0.251
H5	205	22.029	0.042	3922.1	5.9	1.5946	0.0034	63.92	0.34	0.0729	0.0004	8.224	0.047
H5	235	15.067	0.181	4283.4	14.1	1.5891	0.0095	103.14	3.91	0.0742	0.0027	8.381	0.312
H5	255	14.525	0.249	3827.0	32.4	1.5765	0.0133	103.35	2.74	0.0809	0.0016	9.164	0.226
H5	295	90.878	0.800	4474.9	16.1	1.6292	0.0088	21.03	0.38	0.0829	0.0014	9.405	0.166
H5	325	62.874	0.444	4956.1	10.0	1.5440	0.0047	32.16	0.35	0.0846	0.0007	9.605	0.088
H5	350	40.475	0.102	4118.2	6.3	1.6366	0.0025	44.89	0.20	0.0869	0.0003	9.867	0.044
H5	400	10.175	0.037	4008.9	6.0	1.5427	0.0039	162.77	1.00	0.0873	0.0005	9.920	0.060
H5	435	22.518	0.163	3034.6	6.4	1.5809	0.0072	58.76	0.80	0.0892	0.0011	10.147	0.131
H5	457	0.468	0.003	3379.3	6.6	1.5731	0.0048	3080.48	45.72	0.0887	0.0012	10.091	0.147
H5	480	24.588	0.246	3466.1	10.4	1.5740	0.0085	60.39	1.80	0.0880	0.0025	10.011	0.302
H5	498	5.842	0.044	4159.4	9.2	1.5605	0.0051	306.45	3.79	0.0901	0.0009	10.250	0.112
H12	85	6.880	0.053	1436.1	3.6	1.3833	0.0053	2.68	0.06	0.0021	0.0000	0.232	0.005
H12	151	13.918	0.187	1639.5	3.3	1.3877	0.0050	2.84	0.12	0.0041	0.0002	0.447	0.018
H12	221	4.204	0.031	1423.7	2.9	1.3858	0.0053	9.09	0.20	0.0058	0.0001	0.633	0.014
H12	338	1.244	0.010	1031.8	1.8	1.3655	0.0056	41.72	0.88	0.0118	0.0002	1.298	0.026
H12	372	7.560	0.056	1317.4	2.3	1.3718	0.0048	10.79	0.19	0.0137	0.0002	1.505	0.024
H12	391	17.738	0.146	1548.4	3.4	1.3894	0.0055	6.34	0.09	0.0150	0.0002	1.647	0.022
H12	400	18.855	0.152	2684.1	6.6	1.3735	0.0058	9.66	0.17	0.0149	0.0002	1.633	0.027
H12*	450	4.361	0.020	1613.0	2.2	1.3828	0.0010	25.24	0.23	0.0163	0.0001	1.791	0.029
H12	571	20.869	0.163	1768.5	4.5	1.3779	0.0062	9.17	0.15	0.0235	0.0004	2.597	0.040
H12*	585	2.017	0.015	1720.1	2.3	1.3737	0.0010	83.57	1.16	0.0236	0.0003	2.598	0.062
H12	595	23.971	3.140	1917.2	4.4	1.3620	0.0052	16.65	2.19	0.0478	0.0006	5.333	0.069
H12	638	28.087	0.370	2101.8	6.2	1.3419	0.0078	16.88	0.36	0.0526	0.0009	5.887	0.110
H12	660	4.145	0.059	1750.6	3.5	1.3388	0.0051	91.24	1.70	0.0524	0.0007	5.862	0.075
H12*	665	3.032	0.019	1702.0	2.3	1.3406	0.0010	119.25	0.98	0.0525	0.0003	5.850	0.068
H12	744	18.588	0.142	1847.1	4.6	1.3276	0.0060	21.95	0.37	0.0526	0.0008	5.887	0.099
H12	760	9.429	0.085	1728.1	4.2	1.3276	0.0050	41.59	0.57	0.0549	0.0006	6.157	0.070
H12*	780	6.292	0.028	1382.9	1.9	1.3308	0.0009	50.12	0.39	0.0568	0.0004	6.341	0.085
Q5	2	1.647	0.012	448.0	2.2	0.9422	0.0058	3.69	0.19	0.0037	0.0002	0.403	0.021
Q5*	40	2.164	0.012	664.9	1.8	0.9348	0.0007	11.83	0.14	0.0136	0.0002	1.400	0.030
Q5	62	2.665	0.020	478.0	0.9	0.9333	0.0033	14.86	0.24	0.0275	0.0004	3.049	0.048
Q5	140	0.771	0.007	575.0	1.1	0.9162	0.0038	71.97	2.24	0.0341	0.0010	3.789	0.115
Q5	197	0.762	0.009	480.4	1.0	0.9301	0.0058	62.73	1.93	0.0346	0.0010	3.845	0.116
Q5	259	2.973	0.067	533.5	3.4	0.9322	0.0188	21.14	0.94	0.0398	0.0017	4.441	0.196
Q5	340	0.373	0.003	567.5	1.1	0.9151	0.0043	170.14	3.48	0.0398	0.0008	4.435	0.089
Q5	428	2.354	0.021	558.7	1.1	0.9271	0.0046	30.67	0.70	0.0445	0.0010	4.969	0.110
Q5	503	0.575	0.005	604.3	1.3	0.9116	0.0049	152.98	2.97	0.0520	0.0010	5.838	0.107
Q5*	565	3.334	0.022	606.3	1.6	0.9149	0.0010	28.88	0.32	0.0575	0.0005	6.470	0.090
Q5	574	1.213	0.010	595.6	1.3	0.9202	0.0047	82.10	1.91	0.0589	0.0013	6.634	0.156
Q5*	627	1.641	0.009	632.9	1.6	0.9275	0.0008	66.58	0.58	0.0616	0.0005	6.960	0.080
Q5	702	1.625	0.038	681.6	1.6	0.9107	0.0034	83.43	2.66	0.0708	0.0016	8.030	0.180
Q5*	762	0.449	0.003	676.2	1.7	0.9132	0.0009	324.13	3.58	0.0780	0.0008	8.880	0.120
Q5	780	38.520	0.409	800.4	2.3	0.9386	0.0038	5.45	0.13	0.0790	0.0016	8.996	0.195
Q5	860	0.386	0.003	1553.4	3.2	0.9207	0.0036	980.55	13.34	0.0866	0.0010	9.903	0.120
Q5	903	0.932	0.009	1539.5	3.6	0.9086	0.0045	409.59	7.18	0.0891	0.0013	10.210	0.164
Q5	961	0.268	0.002	1790.7	3.4	0.9065	0.0027	1716.60	24.05	0.0926	0.0011	10.623	0.138
S3	149	0.410	0.005	273.6	0.7	1.0412	0.0038	8.91	1.20	0.0038	0.0005	0.418	0.057
S3	245	0.316	0.003	238.3	0.5	1.0380	0.0046	17.09	0.45	0.0068	0.0002	0.746	0.019
S4	10	3.200	0.007	592.8	1.9	1.0839	0.0048	50.17	0.47	0.0806	0.0008	9.163	0.098
S4*	75	1.369	0.008	483.0	1.2	1.0357	0.0027	94.32	0.94	0.0855	0.0011	9.674	0.170
S4	89	1.772	0.013	379.6	1.0	1.0465	0.0046	56.58	0.83	0.0815	0.0011	9.283	0.136
S4	120	1.613	0.013	379.8	0.9	1.0547	0.0053	65.04	1.05	0.0847	0.0012	9.661	0.148

Table 1 (*continued*)

Sample	Depth (mm)	c(Th)		c(U)		(234U/238U)		(230Th/232Th)		(230Th/234U)		Age	
		(ppb)	±	(ppb)	±		±		±		±	(ka)	±
S4	121	1.025	0.010	267.4	0.5	1.0413	0.0049	71.03	1.26	0.0847	0.0013	9.660	0.155
S4*	135	1.046	0.006	416.7	1.1	1.0455	0.0023	107.10	1.21	0.0851	0.0013	9.670	0.100
S4*	168	3.171	0.018	499.3	1.3	1.0385	0.0046	42.40	0.50	0.0859	0.0014	9.760	0.120
S4*	205	2.792	0.014	472.8	1.2	1.0585	0.0031	47.15	0.43	0.0871	0.0011	9.908	0.09
S4*	220	2.223	0.012	489.3	1.2	1.0358	0.0028	60.76	0.61	0.0883	0.0012	9.964	0.168
S4	230	2.660	0.005	409.8	1.1	1.0502	0.0048	44.33	0.45	0.0882	0.0009	10.077	0.120
S4*	395	6.698	0.036	603.0	1.5	1.0370	0.0027	27.44	0.24	0.0974	0.0011	10.864	0.183
S4*	415	4.720	0.025	596.7	1.5	1.0101	0.0033	36.81	0.30	0.0955	0.0010	10.742	0.153
S4*	420	2.676	0.014	548.9	1.5	1.0254	0.0014	59.95	0.54	0.0944	0.0007	10.681	0.122
S4	421	4.498	0.044	583.1	1.3	1.0326	0.0066	39.13	0.86	0.0939	0.0019	10.761	0.234
D1*	312	0.281	0.003	438.9	1.1	1.3367	0.0015	84.93	2.48	0.0135	0.0004	1.480	0.050
D1*	432	0.155	0.001	466.5	1.3	1.3431	0.0033	208.85	3.16	0.0171	0.0002	1.890	0.030
D1*	565	0.153	0.002	450.0	1.2	1.3348	0.0019	235.01	4.45	0.0198	0.0002	2.170	0.050
D1*	665	0.145	0.001	459.2	1.2	1.3431	0.0010	310.46	5.03	0.0241	0.0004	2.670	0.060
D1*	810	0.087	0.001	496.2	1.4	1.3557	0.0023	666.59	7.62	0.0284	0.0003	3.140	0.050
D1*	875	0.373	0.026	465.7	1.2	1.3399	0.0012	16.68	0.24	0.0330	0.0004	3.490	0.060
D1*	960	0.310	0.002	381.8	1.0	1.3427	0.0019	167.28	1.86	0.0335	0.0003	3.720	0.060
D1*	1040	0.386	0.005	356.8	0.9	1.3368	0.0011	143.79	3.54	0.0386	0.0008	4.290	0.110
D1*	1115	0.414	0.002	331.7	0.9	1.3587	0.0039	133.81	1.67	0.0407	0.0005	4.530	0.080

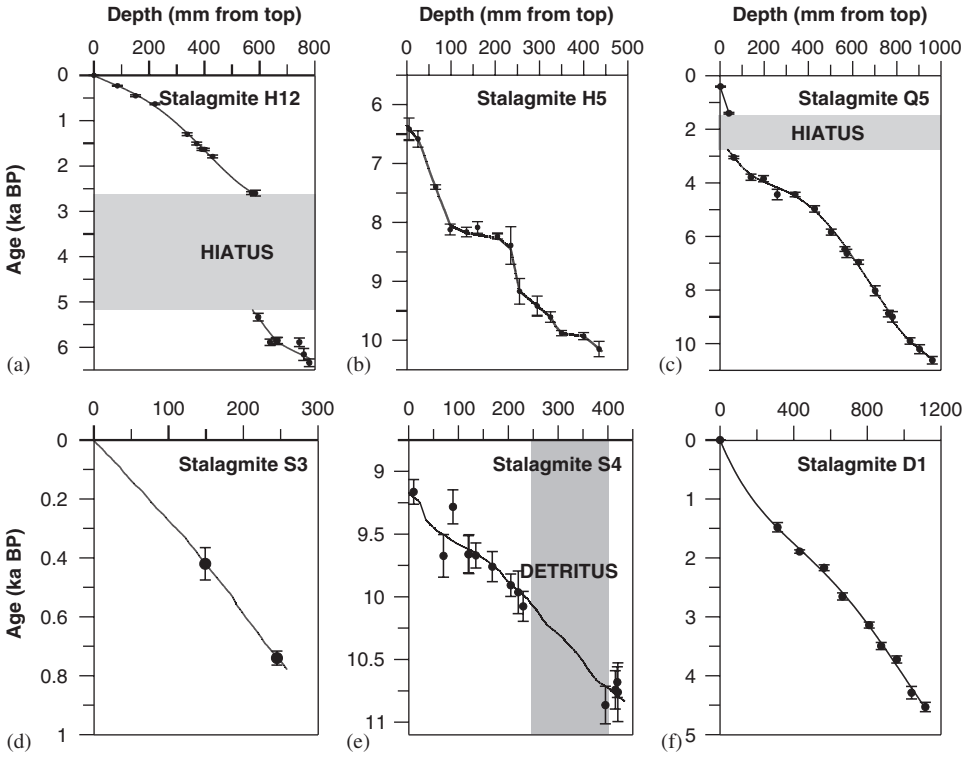

Fig. 3. (a–f) Age versus depth plots for studied stalagmites (see also Table 1). Bold black lines in figures (d) and (e) are based on annual layer counts. The number of counted layers is in good agreement with U–Th ages. Gray shaded area in (a) and (c) mark hiatus. Gray shaded area in Fig. 3 e marks the proportion of S4 for which no reliable Th–U could be obtained due to abundant dust and contamination with ^{232}Th.

For stalagmites S3 and S4 from Kahf Defore the combination of annual layer counts and Th–U dating results in floating but more precise chronologies (Figs. 3d and e). Average growth rates are high and vary between 0.05 and 0.6 mm yr^{-1}. In some cases, detritus corrections were needed when $^{230}Th/^{232}Th$ ratios were high (see Table 1). If necessary, ages were corrected assuming a $^{232}Th/^{234}U$ ratio of 3.8 (see Frank et al., 2000 for details). Detritus corrections were needed for stalagmites S3 and S4 from Kahf Defore (Southern Oman) and stalagmites H5 and H12 from Hoti Cave (Northern Oman). We must, however, emphasize that their chronologies are either confirmed by annual layer counts (S3 and S4, Figs. 3d, e) or by Th–U ages (H5 and H12) for which no or minor detritus correction was needed (see Table 1 for details). Age versus depth plots of all stalagmites show that almost all Th–U ages are in stratigraphic order (Fig. 3a–f), enabling us to establish precise chronologies, with age uncertainties typically varying between 1% and 3% of the absolute age.

4.2. Oxygen isotope profiles

Profiles of $\delta^{18}O$ variations, in which their average temporal resolution varies between 1.5 and 10 years, are shown in Fig. 4. Unfortunately, none of the $\delta^{18}O$ profiles covers the entire Holocene period. Nonetheless the longest profile, derived from stalagmite Q5 (Qunf Cave, Southern Oman), covers most of the Holocene with the exception of two brief periods from 2.6 to 1.4 and 0.4 ka BP to present. The Q5 $\delta^{18}O$-profile is supported by two overlapping profiles from stalagmites S3 and S4 (Defore Cave, Southern Oman). In Northern Oman, the composite $\delta^{18}O$ record is based on stalagmites H12 and H5 from Hoti Cave, which cover the intervals between 10.1 and 5.2 and 2.5 ka BP to present. The Holocene record from Dimarshim Cave on Socotra continuously covers the interval from 4.4 ka BP to present.

$\delta^{18}O$ values in stalagmite H5 (Hoti Cave, Northern Oman) decrease abruptly between 10 and 9.2 ka BP from −4 to −5‰ (VPDB), and then vary around an average value of −4.9‰ (VPDB) from 9.2 to 6.3 ka BP (Fig. 4). An abrupt positive shift to less negative $\delta^{18}O$ occurs at around 6.3 ka BP. In sample H12, $\delta^{18}O$ values for the following interval between 6.3 and 5.2 ka BP average −3.2‰, being approximately 1‰ more negative than present-day $\delta^{18}O$ values. A depositional hiatus exists from 5.2 to 2.5 ka BP. Between 2.5 and present (A.D. 1997) $\delta^{18}O$ values vary by approx. 3‰ around an average value of −2.2‰.

For Southern Oman, stalagmites S4 (Kahf Defore) and Q5 (Qunf Cave) show a simultaneous decrease in $\delta^{18}O$ from −0.8‰ to −2.0‰ and −0.2‰ to −1.3‰, respectively between 10.6 and 9.8 ka BP (Fig. 4). $\delta^{18}O$ values of stalagmite Q5 remain generally low between 9.8 and 7.8 ka BP and then increase gradually from −2.2‰ to almost modern values of −0.9‰ at 2.7 ka BP. As Kahf Defore (~150 masl) is located at lower altitude than Qunf Cave (~650 masl), the overall difference of approximately 0.6‰ in $\delta^{18}O$ between S4 and Q5 can be attributed to the so-called "altitude effect", which is 0.1–0.15‰ per 100 m in Southern Oman (Clark et al., 1987; Fleitmann et al., 2004). The D1 oxygen isotope record from Socotra, the southernmost of all studied sites, covers the last 4.4 ka B.P. and reveals a long-term decrease in $\delta^{18}O$ from values of around −3.0‰ to modern values of −4.2‰ (Fig. 4). All records show distinct decadal to multi-decadal variations in $\delta^{18}O$ of up to 2‰, which are superimposed on the long-term trends.

5. Paleoclimatic significance of oxygen isotope ratios

Based on previously published results from Oman and Yemen, we interpret the oxygen isotope ratios of stalagmite calcite to primarily reflect variations in the amount of rainfall (termed "amount effect"; Dansgaard, 1964; Rozanski et al., 1992), with more negative $\delta^{18}O$ reflecting higher monsoon rainfall (Burns et al., 1998, 2001, 2003; Neff et al., 2001; detailed discussion in Fleitmann et al., 2004). This interpretation is substantiated by isotopic time series of tropical precipitation (Dansgaard, 1964; Rozanski et al., 1992; Johnson and Ingram, 2004) and paleoclimate records from the ASM domain (e.g., Wei and Gasse, 1999; Wang et al., 2001, 2005; Dykoski et al., 2005), which confirm the inverse relationship between $\delta^{18}O$ and the amount of precipitation in regions affected by monsoons. Additional evidence for our interpretation comes from the statistically significant correlation between $\delta^{18}O$ and the thickness of annual bands, which were measured on four stalagmites from Kahf Defore in Southern Oman (Burns et al., 2002; Fleitmann et al., 2004). Numerous studies performed on annually laminated stalagmites (e.g., Genty and Quinif, 1996; Polyak and Asmerom, 2001; Yadava et al., 2004) suggest that the thickness of annual bands is primarily controlled by the drip rate, which in turn closely relates to the amount of precipitation (higher drip rate-higher surface precipitation). In stalagmites from Kahf Defore, more negative $\delta^{18}O$ values (higher precipitation) anti-correlate with thicker growth bands (higher drip rate) and vice versa, with Pearson's correlation coefficients varying between −0.6 and −0.4 (Fleitmann et al., 2004). Although evaporation can affect $\delta^{18}O$ of precipitation, cave seepage water and, thus, speleothem calcite, this process acts in the same "direction" as the "amount effect as evaporation is reduced during intervals of higher precipitation (Burns et al., 1998, 2001; Fleitmann et al., 2004). However, we must emphasize that the effects of evaporation on $\delta^{18}O$ of speleothem calcite were observed in one cave only: viz. Defore Cave. In this cave relative humidity (rH) is relatively low (rH = 92–98%), and even here modern calcite is within 1‰ of the expected equilibrium value (Burns et al., 2002; Fleitmann et al., 2004).

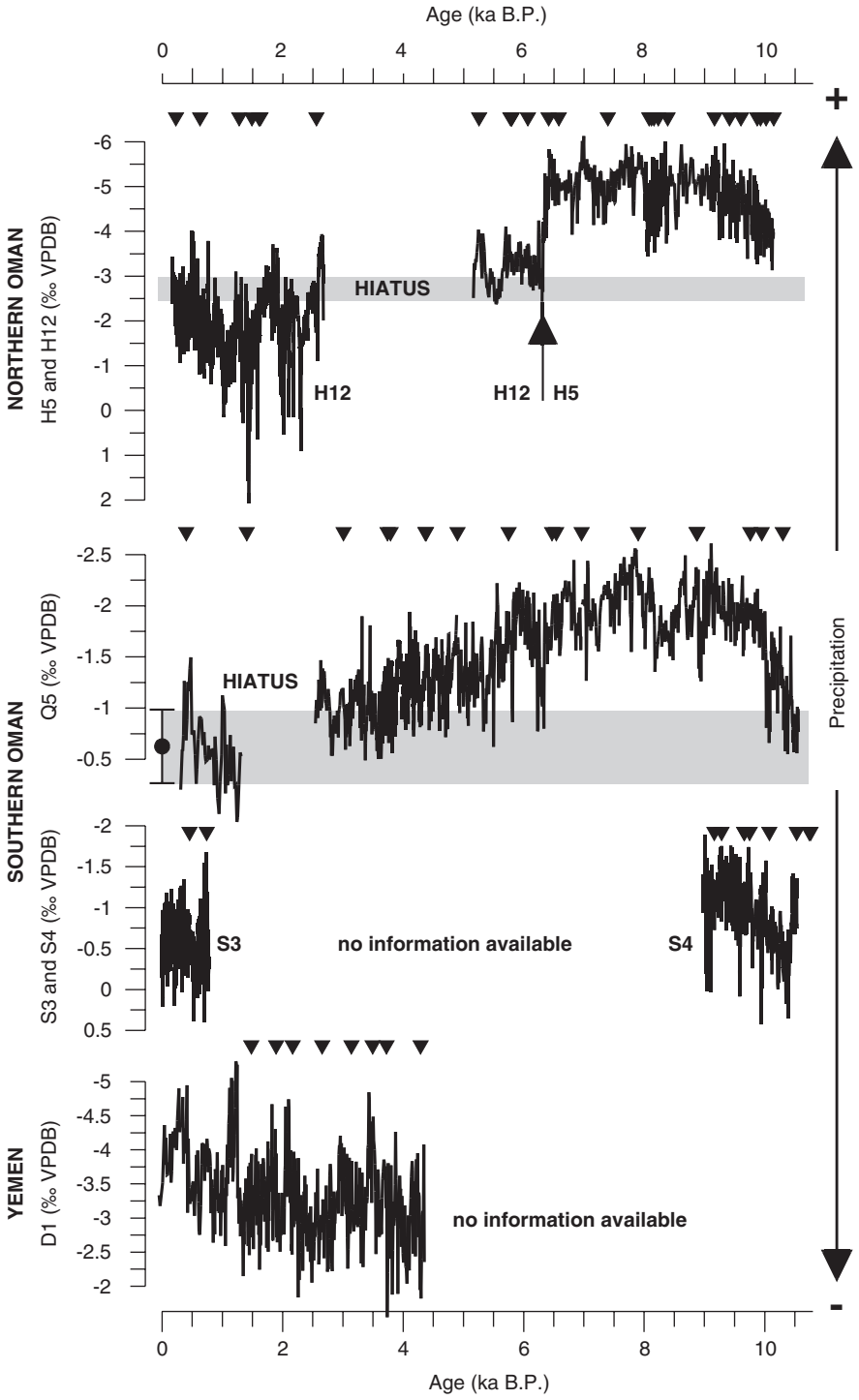

Fig. 4. Oxygen isotope profiles of all studied stalagmites. Dots with error bars and gray-shaded areas mark the isotopic range of modern stalagmites. Black triangles marh Th-U ages.

In addition to the "amount effect", $\delta^{18}O$ values in stalagmites from Northern Oman also reflect shifts in the moisture source over time, viz. from a southern moisture source (Indian Ocean, monsoon and cyclones) during the early to mid-Holocene to a northern moisture source (Eastern Mediterranean, winter depressions) during the late Holocene (Burns et al., 1998, 2001; Fleitmann et al., 2003b). Such a change in the source of moisture is accompanied by a significant positive shift of approximately 2–4‰ in $\delta^{18}O$, as rainfall from the northern moisture source is isotopically enriched compared to rainfall from the southern moisture source (Burns et al., 1998, 2001; Weyhenmeyer et al., 2000, 2002; Fleitmann et al., 2003b).

One important question for the studied sites is whether the amount of monsoon precipitation in Oman is primarily related to the intensity of the ISM or to the latitudinal position of the ITCZ and convective activity within it, or some combination. We propose that both are important controls for the amount of monsoon precipitation for the following two reasons. First, the low-level monsoon winds transport large amounts of moisture from the Southern Indian Ocean, which fuel the convective cells within or along the ITCZ. Second, the release of latent heat during the monsoon months is an important driving force for the intensity of the monsoon (e.g., Webster et al., 1998). From there, the advection of moisture is a major control for the convective activity within or along the ITCZ and, due to the release of latent heat, for the strength of the ISM. Thus, we suggest that the ITCZ and the ISM vary to a certain extent in concert; stronger surface heating during boreal summer in response to greater solar insolation would pull the ITCZ northward and intensify monsoon circulation due to a greater surface heating of the Eurasian landmass and the resultant enhanced land-sea thermal contrast (Webster et al., 1998). Moreover, stronger monsoon circulation would enhance cross-equatorial transport of moisture, which in turn intensifies convection within the summer ITCZ and ISM circulation due to the greater release of latent heat. This positive feedback mechanism would lead to higher monsoon precipitation in Oman and other areas located close to the summer ITCZ. Although there are no long-term instrumental data available to verify the accuracy of the proposed and possibly oversimplified relationship, there is a strong correlation between wind strength over the Arabian Sea and monsoon precipitation over India and Southeast Asia (Ju and Slingo, 1995; Halpern and Woiceshyn, 2001), with deficit rainfall over west India being associated with a weaker Somali Jet. It is plausible that this linkage may also act on longer time-scales ranging from decadal to centennial.

An area that is particularly sensitive to changes in the mean latitudinal position of the ITCZ and convective activity within it is Southern Oman. Here, convective cloud development is currently prevented by a temperature inversion located over Southern Oman (Findlater, 1969; Narayanan and Rao, 1981; Sirocko et al., 1991; Fig. 5a), whereas the height of this temperature inversion is dynamically linked to the mean latitudinal summer position of the ITCZ and to the monsoon wind pattern over Southern Arabia. A northward shift of the ITCZ into the Arabian Peninsula, as indicated by lacustrine sediments (McClure, 1976; Lézine et al., 1998) and dune deposits (Bray and Stokes, 2004), would lift the height of the temperature inversion, leading to stronger convective cloud development and higher monsoonal rainfall over Southern Oman (Fig 5b). Hence, the Q5 $\delta^{18}O$ time series is very sensitive to variations in the latitudinal summer position of the ITCZ over the Arabian Peninsula. Due to the "amount effect" (Dansgaard, 1964; Rozanski et al., 1992), $\delta^{18}O$ values of precipitation become more negative (depleted).

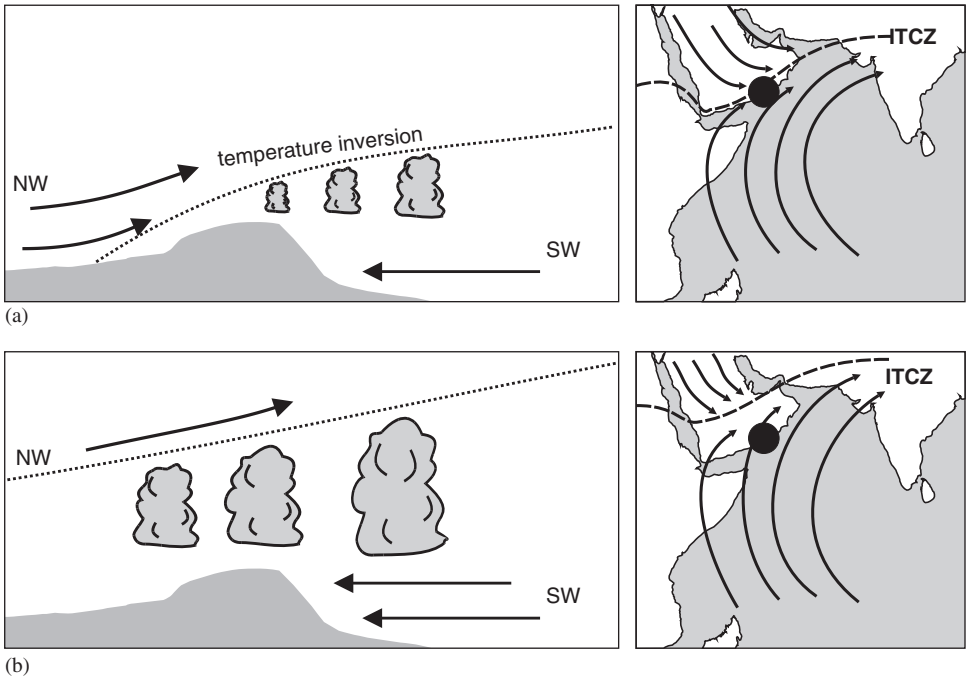

Fig. 5. (a) Schematic figure of modern summer circulation pattern over Southern Oman. The black dot shows the location of Qunf Cave. The black dotted line shows the position of the temperature inversion and the black dashed line the location of the ITCZ. (b) Schematic figure of summer circulation pattern at around 7 ka BP.

6. Holocene ITCZ and monsoon dynamics in Oman as revealed by stalagmite $\delta^{18}O$-profiles

6.1. Early Holocene (11–8 ka BP)

The stalagmite $\delta^{18}O$ profiles indicate a rapid increase in ISM precipitation between ~10.6 and 9.7 ka BP in Southern Oman and ~10.1 and 9.2 ka BP in Northern Oman (Fig. 6). This is good agreement with Arabian Sea upwelling records (Sirocko et al., 1993; Overpeck et al., 1996; Jung et al., 2002; Ivanochko et al., 2005) and lake levels from India (e.g., Enzel et al., 1999). Although some of these records show a two-step intensification of the monsoon at ~13–12.5 and 11–10 ka BP (e.g., Sirocko et al., 1993; Overpeck et al., 1996; Ivanochko et al., 2005), there is currently no speleothem evidence in Oman for an onset in monsoon precipitation prior to ~10.6 (Fleitmann et al., 2003a). This may indicate that the ITCZ and the associated rain belt remained south of Oman prior to ~10.6 ka BP.

In Oman the onset and increase in monsoon precipitation lags the peak in summer (June) insolation (Berger and Loutre, 1991), the major driver of the ISM on orbital timescales (Prell and Kutzbach, 1987; Clemens et al., 1991), by approximately 1.5 ka (Fig. 6). This delayed response of the ISM to insolation forcing is also well documented in previously published paleoclimate records from this area and there is now a broad consensus that glacial boundary forcing, such as North Atlantic air temperatures and Eurasian snow cover, suppressed the effects of solar insolation forcing during the last deglaciation until the beginning of the Holocene (e.g., Prell and Kutzbach, 1992; Sirocko et al., 1993; Overpeck et al., 1996; Gupta et al., 2003; Fleitmann et al., 2003a, b; Dykoski et al., 2005).

The H5, S4 and Q5 $\delta^{18}O$-profiles also closely resemble the GRIP, NGRIP and DYE-3 $\delta^{18}O$-records on multi-decadal timescales (Johnsen et al., 2001; Fig. 6). Taking age uncertainties of between 100 and 200 years for each record into account, colder North Atlantic air temperatures (more negative $\delta^{18}O$ in the ice core $\delta^{18}O$ time series) tend to coincide with reduced monsoon precipitation (more positive $\delta^{18}O$ in the stalagmite) and vice versa. In particular two distinct climatic events at ~8.2 ka BP (so-called "8.2 ka cold event"; Alley et al., 1997) and ~9.2 ka BP stand out in

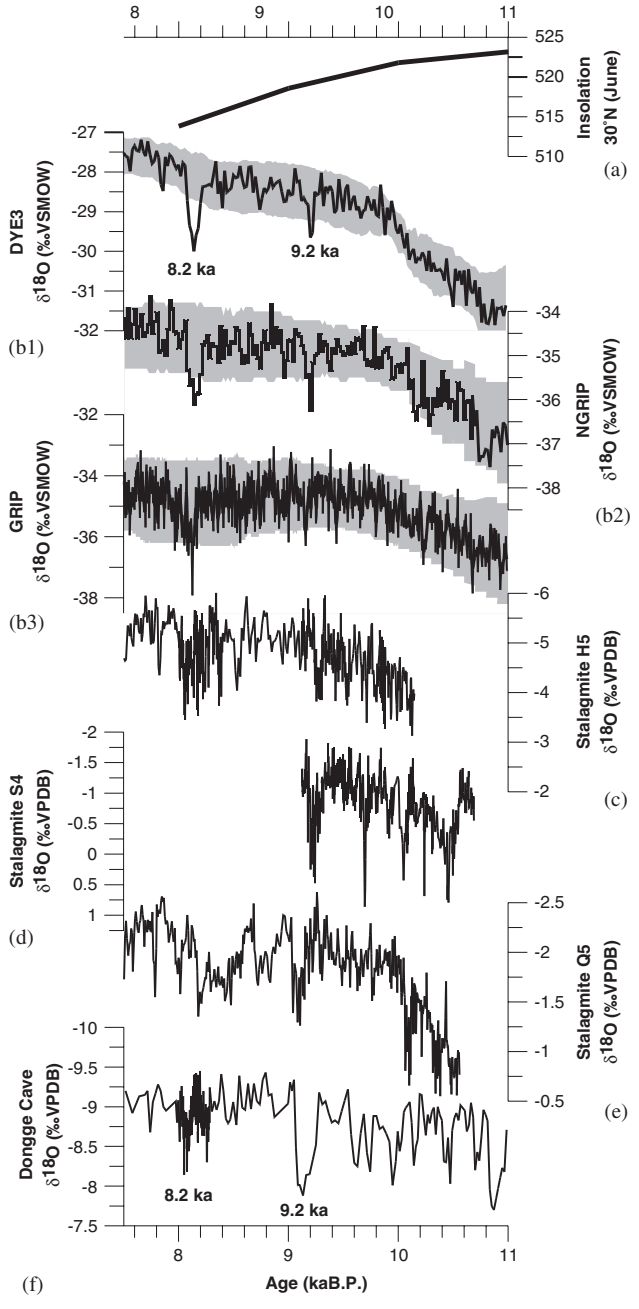

Fig. 6. (a) Summer insolation curve (June) for 30°N (Berger and Loutre, 1991). (b1–3) DYE 3, GRIP and NGRIP $\delta^{18}O$ ice core records (Dansgaard et al., 1993; Johnsen et al., 2001). In order to test the statistic significance of the 9.2 and 8.2 ka events, we constructed a robust 95% confidence band (shaded) as follows. A running window ($2k+1$ points) was used to calculate the median as an estimate of the time-dependent background that is robust against the presence of extremes. The median of absolute distances to the median (MAD) was calculated as a robust estimate of the time-dependent variability (Mudelsee, 2006). The 95% confidence band is given by median ± 2.96 MAD. A normal distribution with standard deviation σ has MAD $= 1.48\sigma$ and a 95% confidence interval of $\pm 2\sigma$. We selected following values of k for the unevenly spaced time series to obtain average window widths in the order of 600–1000 years, that is, to permit millennial-scale background and variability variations. NGRIP, $k = 25$; GRIP, $k = 89$; DYE-3, $k = 25$. Calculations were made using the software CLIM-X-DETECT (Mudelsee, 2006). (c–e) Stalagmite $\delta^{18}O$ records from northern (H5) and southern Oman (Q5 and S4). Note, the H5 time series differs from that presented by Neff et al. (2001) as it is not tuned to the tree ring based ^{14}C record (Stuiver et al., 1998). (f) $\delta^{18}O$-profile of stalagmite DA from Dongge Cave, China (Dykoski et al., 2005; see Fig. 1 for location). The increase in ISM and ASM precipitation clearly lags behind summer insolation by approximately 1.5 ka. Notable weak ISM and ASM events, such as at 9.2 and 8.2 ka BP, correlate with cold intervals in ice cores from Greenland.

all $\delta^{18}O$ time series shown in Fig. 6, including a recently published stalagmite-based ASM record from Dongge Cave in China (Dykoski et al., 2005). While there is evidence that the 8.2 ka cold event was triggered by a catastrophic outburst from Lake Agassiz through the Hudson strait into the northern North Atlantic (Barber et al., 1999), the cause of the 9.2 ka event is not yet fully known. However, this event coincides with an outburst of meltwater at ~9.17 ka BP, although the volume of meltwater released in this outburst was significantly smaller than that released at ~8.2 ka (~0.27 Sv versus 5.1 Sv (1 Sverdrup $= 1 \times 10^6\,m^3\,s^{-1}$) Teller and Leverington, 2004). Nevertheless, the meltwater outbursts at 9.2 and 8.2 ka BP were probably sufficient to weaken the thermohaline circulation, which then resulted in cooler North Atlantic air temperatures, as are well documented in three Greenland ice cores (DYE 3, NGRIP, GRIP; Johnsen et al., 2001; Fig 6). The resultant winter cooling and associated enhanced Eurasian snow cover weakened monsoon circulation via the well-known snow cover-monsoon linkage (e.g., Barnett et al., 1988). Greater extent of snow cover over western Eurasia affects monsoon circulation, as spring heating of the Eurasian landmass is reduced due to higher albedo and higher energy consumption to melt the excess snow (Barnett et al., 1988; Ye and Bao, 2001). This reduction in surface heating of the Tibetan plateau during the following summer then leads to a decreased land-sea pressure gradient and weaker summer monsoon circulation. Likewise, the resultant reduced cross-equatorial transport of moisture by low-level monsoon winds further reduces convective activity within the ITCZ, leading to reduced precipitation in Oman and China (Fig. 6).

An interesting feature in all speleothem-based monsoon time series shown in Fig. 6 is the presence of two distinct $\delta^{18}O$ excursions at around 8.2 ka BP, while there is only one $\delta^{18}O$ anomaly at $\sim 8.18 \pm 0.04$ ka BP in the DYE-3, NGRIP and GRIP ice cores from Greenland. In H5 (Hoti Cave, Northern Oman) and Q5 (Qunf Cave, Southern Oman) both events are centered at 8.17 and 8.06 ka BP and 8.19 and 8.02 ka BP, respectively. This timing is consistent with two anomalies centered at 8.26 ± 0.06 and 8.08 ± 0.07 ka BP in a well-dated stalagmite record from Dongge Cave in China (Fig. 6; Dykoski et al., 2005). Due to chronological uncertainties, however, it remains unclear which of the two monsoon anomalies relate to the 8.2 ka cold event.

To summarize, the $\delta^{18}O$-profiles suggest a rapid northward displacement in the mean latitudinal position of the summer ITCZ and the belt of maximum monsoon precipitation between ~10.6 and ~9.2 ka BP, lagging behind maximum solar insolation by approximately 1.5 ka. Decadal to multi-decadal intervals of reduced monsoon precipitation tend to coincide with cooling events in the North Atlantic, indicating that the dynamics of the ITCZ and ISM and ASM are strongly influenced by northern North Atlantic climate variability.

6.2. Middle to Late Holocene (~8 ka BP—present day)

In Southern Oman, monsoon precipitation increases again shortly after the 8.2 ka cold event, peaks between ~7.9 and 7.6 ka BP and then decreases gradually towards present (Fig. 4). A major decrease in monsoon precipitation, indicated by an abrupt positive shift of 1‰ to 3‰ in $\delta^{18}O$ in the H5 (Hoti Cave) and Q5 (Qunf Cave) time series, occurs at ~6.3 ka BP simultaneously in Northern and Southern Oman (Figs. 4 and 7). In Hoti Cave (Northern Oman) this shift in $\delta^{18}O$ results from the southward retreat in the mean latitudinal position of the summer ITCZ and the associated monsoon rain belt, going along with a shift from a southern (Indian Ocean) to a northern moisture source (Mediterranean) and a change in the seasonality of precipitation, viz. from summer to winter precipitation (Fleitmann et al., 2003b; Fig. 7). Between ~6.3 and 5.2 ka BP stalagmite H12 $\delta^{18}O$ values vary around a mean of −3‰ and are only slightly more negative than those of modern and late Holocene stalagmites from Hoti Cave (Fig. 4). Such intermediate $\delta^{18}O$ values most likely indicate that the mean latitudinal position of the summer ITCZ and the ISM rain belt were mainly located south of Hoti Cave (23°N) after ~6.3 ka BP, although we can not completely exclude that ISM precipitation reached Northern Oman occasionally. Qunf Cave in Southern Oman (17°N), however, was still affected by the ISM after ~6.3 ka BP (as it is today) and Q5 $\delta^{18}O$ values continuously decrease until ~2.7 ka BP when there was an interruption in stalagmite deposition (Figs. 3c and 4). The specific cause for the hiatus between ~2.7 and 1.4 ka BP is uncertain, as it could have been caused by a temporary blocking of the fissure-feeding stalagmite Q5 or a significant drop in monsoon precipitation. The latter explanation, however, seems to be more likely as the cessation of growth coincides with a marked arid interval on the Southern Arabian Peninsula, as indicated by a period of dune deposition in the Liwa region (Bray and Stokes, 2004) and the Wahiba Sands (Radies et al., 2004) in the United Arab Emirates and Oman, respectively (Fig. 7).

The long-term gradual change in the Q5 $\delta^{18}O$ profile indicates a continuous southward retreat of the summer ITCZ, a weakening in ISM strength and reduction in convective activity within or along the ITCZ in response to decreasing summer insolation (Fig. 8; Fleitmann et al., 2003a). In contrast to the gradual decrease in ISM precipitation recorded in stalagmite Q5 from Southern Oman, the D1 stalagmite $\delta^{18}O$ record from Socotra shows a long-term increase in inter-monsoon (spring and autumn) precipitation, as indicated by a long-term decrease in $\delta^{18}O$ since ~4.4 ka BP (Figs. 4 and 7). This anti-phase behavior between Southern Oman and Socotra seems to be apparent not only on millennial but also on multi-decadal timescales. In order to better reveal the anti-correlation between precipitation in Southern Oman and Socotra in greater detail, we compared the overlapping $\delta^{18}O$ profiles

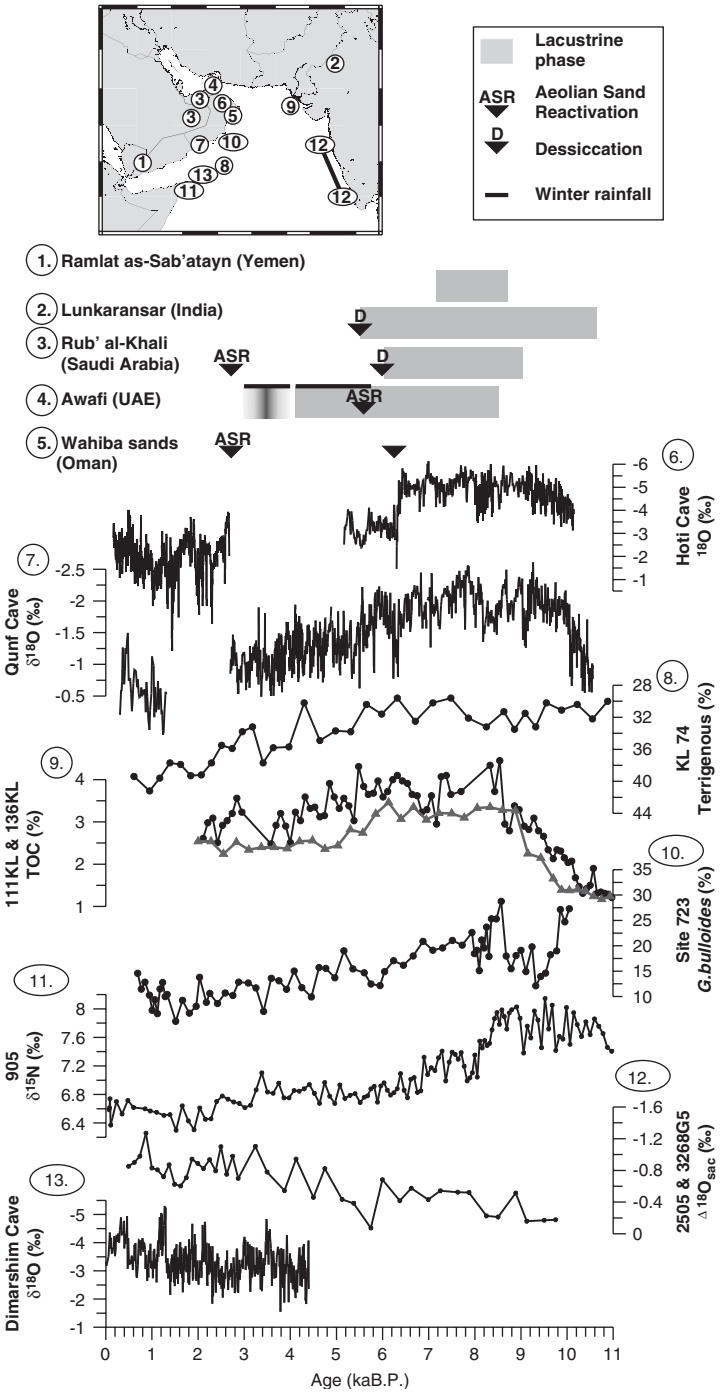

Fig. 7. Compilation of records from the ISM domain. Location of all records is shown in map on top. **1**. Ramlat as Sab'atayn (Lézine et al., 1998); **2**. Lunkaransar (India; Enzel et al., 1999); **3**. Rub' al-Khali (Saudi Arabia; McClure, 1976); **4**. Awafi (United Arabian Emirates; Parker et al., 2004); **5**. Wahiba Sands (Oman; Radies et al., 2004); **6**. Hoti Cave (Northern Oman; Neff et al., 2001; this study); **7**. Qunf Cave (Southern Oman; Fleitmann et al., 2003a, b); **8**. KL74 (Northern Arabian Sea, Sirocko et al., 1993); **9**. 111KL and 136KL (Northern Arabian Sea; Schulz et al., 1998); **10**. ODP site 723 (Northern Arabian Sea, Gupta et al., 2003); **11.** 905 (Western Arabian Sea, Ivanochko et al., 2005); **12**. 2505 and 3268G5 (Eastern Arabian Sea, Sarkar et al., 2000); **13**. Dimarshim Cave (Socotra, this study).

of stalagmites Q5 and D1 (Fig. 9). This comparison shows a visible anti-correlation, with higher monsoon precipitation in Southern Oman coinciding with lower intermonsoon (spring/autumn) precipitation on Socotra. Because the onset and termination of the summer monsoon on Socotra determines the end of the spring and start of the autumn precipitation season respectively (as it is in Eastern Africa; Camberlin and Okoola, 2003), it is conceivable that

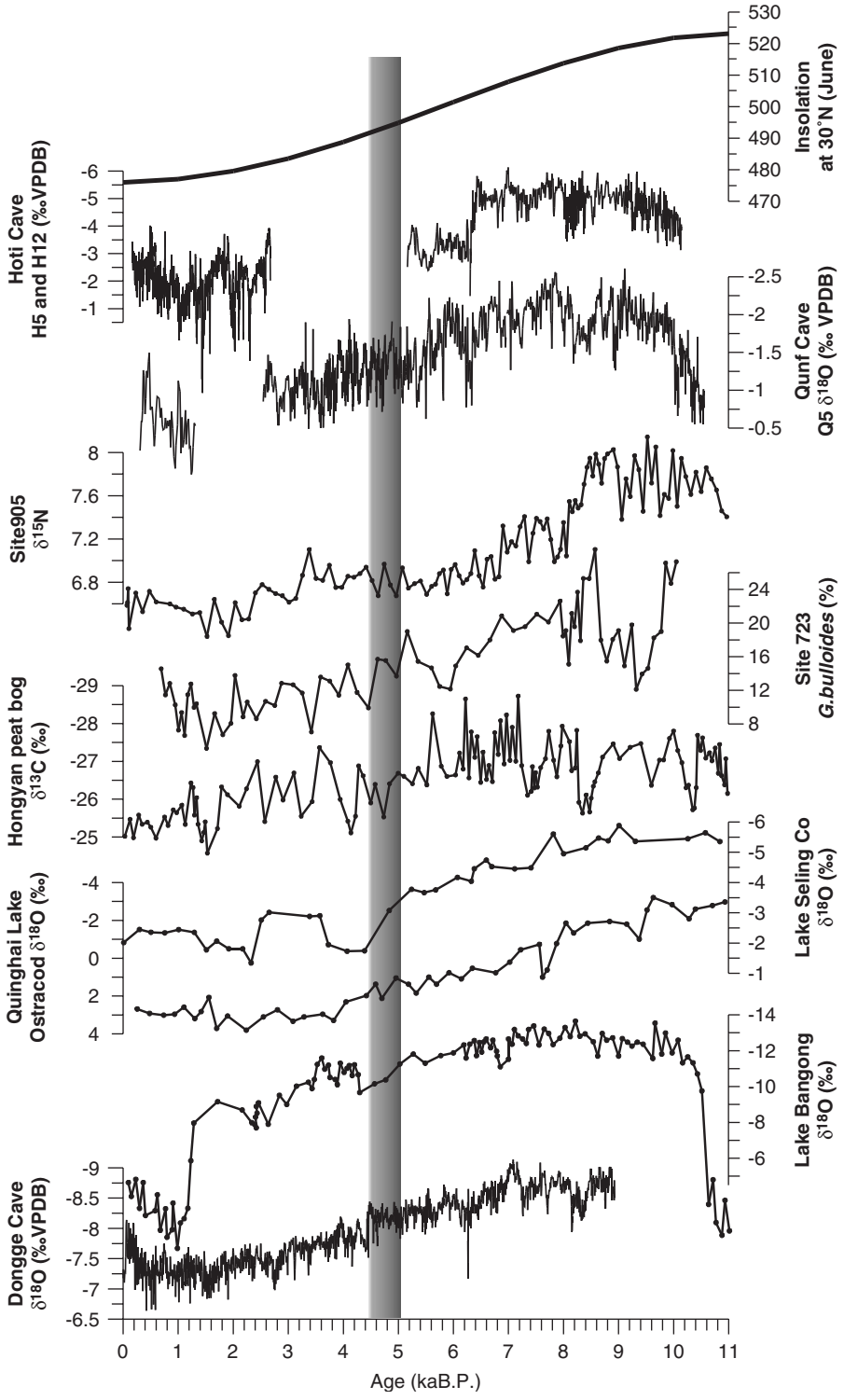

Fig. 8. Comparison between stalagmite and other high-resolution proxy records from the ISM domain (see map for location). (a) June insolation curve for 30°N (Berger and Loutre, 1991). (b) Composite $\delta^{18}O$ record (stalagmites H5 and H12) from Hoti Cave in Northern Oman (Neff et al., 2001) and (c) from Qunf Cave (Q5; Fleitmann et al., 2003a, b). (d) $\delta^{13}C$ time series of *Carex mulieensis* remains from a Tibetan peat bog (Hong et al., 2003). (e) Abundance of *G. bulloides* in a core offshore Oman (Gupta et al., 2003). (f) Stalagmite $\delta^{18}O$ record from Dimarshim Cave on Socotra. (g) Variations in $\delta^{18}O_{sac}$ in a core (3268G5) offshore the west coast of India (Sarkar et al., 2000). $\delta^{18}O_{sac}$ is defined as the difference in $\delta^{18}O$ between cores 3268G5 and 2505 (see map for location).

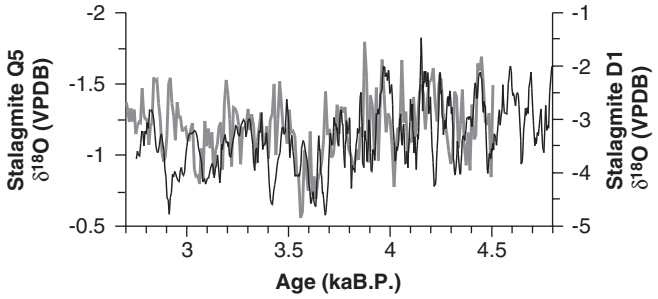

Fig. 9. Comparison between overlapping $\delta^{18}O$-profiles from Southern Oman (Q5, Qunf Cave; black line) and Socotra (D1, Dimarshim Cave; gray line). Note the strong visible anti-correlation between D1 and Q5.

a gradual shortening in the length of the summer monsoon season resulted in an extension of pre- and post-monsoon rainy season precipitation on Socotra. Interestingly, results of climate model simulations tend to support our interpretation of a progressive shortening in the duration of the ISM season since at ~7 ka BP (Bush, in press). Based on archeological evidences from northern India, Gupta (2004) also suggests that a longer early Holocene monsoon season and the resultant excess of moisture in the post-summer months might have provided, in addition to winter monsoon rains, enough moisture to enable a winter crop in the Indus Basin. Therefore, decreasing insolation forcing might have affected not only the mean latitudinal position of the summer ITCZ and intensity of the ISM but also the length of the monsoon season. A later advance and earlier retreat of the ITCZ in spring and autumn, respectively would lead to an on average shorter monsoon season over Southern Oman. If the movement of the ITCZ took place more slowly, a second effect would be a longer spring/autumn rainfall season over the northern Indian Ocean and Socotra, respectively. Provided that our interpretation is correct, our results should have far-reaching consequences for the interpretation of many monsoon proxy records in the ISM and other monsoon domains, as most paleoclimate time series are commonly interpreted to reflect overall monsoon intensity, but not the duration of the monsoon season.

7. Comparison to paleoclimate records from the Indian and East Asian monsoon domains

As mentioned in the introduction, the nature and timing of the weakening of the ISM and ASM are still controversial and at least two hypotheses exist: The ISM and ASM weakened (1) abruptly between ~4.5 and 5.0 ka BP (Morrill et al., 2003) or (2) gradually since the beginning of the middle Holocene (Overpeck et al., 1996; Gupta et al., 2003; Fleitmann et al., 2003a; Ivanochko et al., 2005; Wang et al., 2005). To demonstrate that monsoon strength weakened gradually in response to slow changes in summer insolation, we compared our speleothem records with other ISM and ASM proxy records (Figs. 7 and 8). In general, there are only few records, which have a sufficiently high temporal resolution and length to permit a more detailed comparison to our stalagmite $\delta^{18}O$ profiles. Records fulfilling these two basic requirements are displayed in Figs. 7 and 8 (see also Fig. 1 for their location).

Terrigenous content in marine core KL74 from the Northern Arabian Sea reflects continental humidity, with higher eolian dust input during more arid climate intervals (Sirocko et al., 1993; Leuschner and Sirocko, 2000). Two marine records from upwelling regions in the Arabian Sea, a nitrogen isotope record from the Somali margin (core 905; Ivanochko et al., 2005) and a *Globigerina bulloides* record from Oman margin (site 723; Gupta et al., 2003), reflect monsoon wind-driven upwelling and are therefore an indicator for the strength of ISM winds. Although not directly located in an upwelling area, cores 111KL and 136KL from the continental margin off Pakistan reflect ISM wind strength, with high contents of total organic carbon being associated with enhanced upwelling in the Northern Arabian Sea (Schulz et al., 1998). Finally, we included two marine records (cores 2505 and 3268G5) from the eastern Arabian Sea (Sarkar et al., 2000; Fig. 7). In these two records oxygen isotope values of *Globigerinoides sacculifer*, expressed as the difference in the isotopic composition ($\delta^{18}O_{sac}$) between both sites, are interpreted to be a proxy for the evaporation–precipitation (E–P) balance and surface water salinity, respectively; more negative $\delta^{18}O_{sac}$ values reflect higher monsoon precipitation and enhanced river runoff from the southern tip of India (Sarkar et al., 2000). Two marine records from the Pakistan margin, an annually laminated core (von Rad et al., 1999) and a highly resolved *Globigerinoides ruber* $\delta^{18}O$ record (Staubwasser et al., 2002, 2003), were—despite their temporal resolution and good chronology—not included in this comparison as their middle to late Holocene sections also reflect variations in winter precipitation (Staubwasser et al., 2003; Lũckge et al., 2001). Important to note, although marine records from the Arabian Sea have chronological uncertainties due to varying surface reservoir ages (Staubwasser et al., 2002) and a low temporal resolution, it is still possible to compare the general millennial-scale pattern with confidence.

Based on the ISM records displayed in Fig. 7 the following general picture emerges. In contrast to the abrupt change in ISM precipitation recorded in Northern Oman (Hoti Cave) at ~6.3 ka BP and other more northerly sites (Fig. 7), all ISM proxy records reveal an almost gradual decrease in monsoon wind strength (core 905, site 723, 111KL and 136KL, see Fig. 1 for location) and precipitation (Qunf Cave and KL74) since the middle Holocene (Fig. 7). Records closer to the equator, on the other hand, reveal a long-term increase in monsoon (cores 2505 and 3268G5) and inter-monsoon precipitation (Dimarshim Cave, Socotra) (Fig. 7), consistent with our idea of a

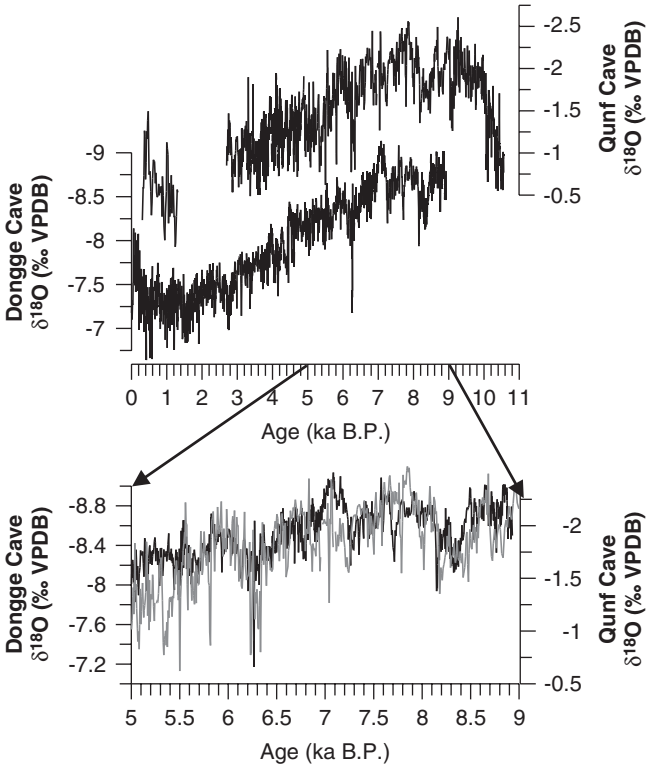

Fig. 10. (a) Detailed comparison between two stalagmite records from Southern Oman (Q5; Qunf Cave) and China (DA, Dongge Cave). (b) Detailed comparison of the early-mid Holocene sections of Q5 (gray line) and DA (black line).

gradual southward migration of the summer ITCZ and monsoon rainfall belt, and a shortening of the summer monsoon season. Importantly, none of the records displayed in Fig. 7 shows clear evidence for a major transition in ISM intensity and precipitation between ~5 and 4.5 ka BP, contradicting the results presented by Morrill et al. (2003). However, we must emphasize that Morrill et al. (2003) found this abrupt mid-Holocene transition in only two records from the ISM domain (for details see Fig. 5D in Morrill et al., 2003), and three of the most recently published records, viz. those from Qunf Cave (Fleitmann et al., 2003a), the Oman (Gupta et al., 2003) and Somali margins (Ivanochko et al., 2005), could not have been included as they were not available to the authors at the time of their analyses.

An abrupt and synchronous mid-Holocene weakening in summer monsoon intensity is also not evident in continental monsoon records from the ASM monsoon domain (Fig. 8), such as the Hongyan peat bog (Hong et al., 2003), Lake Selin (Gu et al., 1993; Wei and Gasse, 1999), Lake Bangong (Fontes et al., 1996), Lake Quinghai (Lister et al., 1991) and Dongge Cave (Wang et al., 2005) isotopic records (see Fig. 1 for location). Although a short-lived reduction in monsoon precipitation between 5 and 4.5 ka BP is visible in some monsoon records, such as the Lake Bangong (Fontes et al., 1996) and Lake Selin records (Gu et al., 1993; Wei and Gasse, 1999), this climatic deterioration is clearly superimposed on a gradual long-term trend. The detailed comparison between stalagmite Q5 (Qunf Cave) from Southern Oman and stalagmite DA (Dongge Cave) from China reveals a very high degree of similarity in both long- and short-term changes in monsoon precipitation (Fig. 10). The monsoon anomaly at 6.3 ka BP is apparent in both stalagmite time series. This high correlation is remarkable as both caves are several thousand kilometers apart (Fig. 1) and underlines that the highly resolved Q5 and DA monsoon proxy records cannot be significantly biased by local climatic effects.

To sum up, none of the most recently published and comprehensive monsoon records (Gupta et al., 2003; Fleitmann et al., 2003a, b; Ivanochko et al., 2005; Dykoski et al., 2005; Wang et al., 2005) shows evidence for an abrupt and widespread change in monsoon intensity during the mid-Holocene (Figs. 7 and 8). This poses the question why some monsoon records suggest an abrupt shift in monsoon precipitation and wind strength while others do not. Because of the gradual southward migration of the ITCZ and the associated monsoon rain belt the timing and nature of the middle to late Holocene humid–arid transition depends on the geographical position of the monsoon proxy record (Fleitmann et al., 2003a). An abrupt humid–arid transition may occur in a particular record as soon as the mean latitudinal position of the ITCZ and the associated summer monsoon rainfall belt are displaced south of the study site, as, for instance, indicated by the abrupt isotopic shift at ~6.3 ka BP in the composite Hoti Cave stalagmite record from Northern Oman, a lacustrine record from the Emirates (Parker et al., 2004) and the Lunkaraskar lacustrine record from Northern India (Enzel et al., 1999) (Fig. 7). Supporting evidence for this assumption comes from a detailed analysis of lake level and loess records from across China (An et al., 2000; He et al., 2004), which show that the belt of maximum ASM precipitation shifted from the northwest to the southeast across China over the course of the Holocene and, as a result, the timing of the onset and termination of the Holocene climatic optimum is asynchronous (An et al., 2000; He et al., 2004). It is also conceivable that abrupt changes in some monsoon proxy records could have resulted of a non-linear response of the geologic record to subtle changes in the amount of precipitation. This is most likely true for lacustrine records in tropical and minor reduction in precipitation due to an average shorter monsoon season or higher variability in precipitation can, by altering the P–E balance from positive to negative, induce a fast and abrupt drop in lake level or even desiccation of the lake (e.g., Bradley, 1999; Gasse et al., 2000). In this case the observed abrupt shift in the lake level or isotopic composition does not necessarily relate to a major and abrupt weakening in monsoon intensity. Therefore, one must consider that abrupt changes in

monsoon proxy records may relate to a shift in the mean latitudinal position of the ITCZ, a change in monsoon circulation or an archive-specific response to a rather subtle change in precipitation. Based on our own and most recently published data, we suggest that the mean summer ITCZ gradually retreated southward and the ISM weakened continuously since approximately 8–7 ka BP (Figs. 7 and 10). Not surprisingly, due to the progressive latitudinal southward shift of the summer ITCZ precipitation increased in the southern part of the Indian subcontinent, as indicated by decreasing salinity (increased freshwater input) at the southern tip of India (Sarkar et al., 2000; Fig. 7) despite the overall weakening in ISM intensity.

Overall, there is now mounting evidence that latitudinal shifts in the mean position of the ITCZ due to changes in insolation affect precipitation throughout the tropics (e.g., Haug et al., 2001; Maslin and Burns, 2000). Taken together, proxy records throughout the northern tropics suggest that post-glacial to modern precipitation patterns are controlled, probably on a global scale, by the gradual southward migration of the ITCZ and gradual weakening of the monsoons in response to orbitally induced decreasing summer insolation.

8. Conclusions

1. The comparison of Holocene stalagmite-based oxygen isotope profiles from Oman and Yemen (Socotra), the caves are located along a transect from 12 to 23°N, provides a new and more detailed view of the spatial and temporal variability of precipitation in the western part of the ISM domain.
2. During the early Holocene (10.5–9.5 ka BP) the mean latitudinal position of the summer ITCZ advances rapidly northward. However, convection within the ITCZ and ISM intensity is, despite orbitally induced maximum solar insolation, suppressed by glacial boundary conditions. Short-term ($10–10^2$ yr) changes in ISM intensity correlate well with high-latitude temperature variations recorded in Greenland ice cores, with reduced (enhanced) convection and lower (higher) ISM intensity being associated with cooler (warmer) high-latitude air temperatures.
3. From 7.8 ka BP to present the mean summer ITCZ continuously migrated southward and ISM intensity and precipitation decreased gradually in response to solar insolation. Furthermore, there is some evidence for a long term shortening of the summer monsoon season. Although abrupt events are apparent in all monsoon records, these events have a short duration and are clearly superimposed on a general long-term gradual trend. This suggests that there is no major abrupt weakening in ISM intensity between 5 and 4 ka BP. Rather, abrupt events detected in various lake records from the ISM domain can be best explained by either a non-linear archive-specific response to fluctuations in precipitation and/or simply by the geographical position. Monsoon records from key-areas in the ISM and ASM domain, such as from Southern Oman (Qunf Cave) or China (Dongge Cave; Wang et al., 2005), clearly demonstrate that the summer ITCZ retreated continuously southward and the ISM weakened gradually in response to decreasing orbital-induced solar insolation.
4. During the late-Holocene, the observed anti-correlation between monsoon precipitation in Southern Oman and inter-monsoon (spring/autumn) precipitation on Socotra possibly reveals that the mean seasonal cycle of the ISM has also changed in response to insolation forcing. Our data demonstrate a shortening in the length of the monsoon season in response to decreasing solar insolation. Together with the progressive shortening of the ISM season and gradual southward retreat of the summer ITCZ, the total amount of monsoon precipitation decreased in those areas located at the northern fringe of the ISM domain, but increased in areas closer to the equator.

Taken together, our results demonstrate that variations in monsoon precipitation resulted by changes in the mean latitudinal position of the ITCZ, the intensity of summer monsoon circulation and length of the monsoon season.

Acknowledgments

We thank Dr. Hilal Mohammad al Azri, Oman Ministry of Industry and Commerce for his support during fieldwork. We gratefully acknowledge the encouragement and assistance by the Environmental Protection Authority (EPA), especially Dr. Mohammed Sayeed Mashgary (President), Mr. Mahmood Shedaiwah, (Deputy), Mr. Abdul Rahman F. Al-Eryani (Manager Socotra Project, EPA) and his team. We would also like to thank Mr. Salem Daheq and his staff in the Socotra EPA office for their support during fieldwork on Socotra. We thank Diego Sanz for caving assistance. Finally, we thank Kathleen B. Johnson and James Russel for helpful comments on an earlier version of this manuscript. This work was supported by the Swiss National Science Foundation (Grant nos. 2021-52472.97 and 2000-059174.99) and the National Science Foundation of the United States (ATM-0135542).

References

Alley, R.B., Mayewski, P.A., Sowers, T., Stuiver, M., Taylor, K.C., Clark, P.U., 1997. Holocene climatic instability: a prominent, widespread event 8200 yr ago. Geology 25, 483–486.

An, Z.S., Porter, S.C., Kutzbach, J.E., Wu, X.H., Wang, S.M., Liu, X.D., Li, X.Q., Zhou, W.J., 2000. Asynchronous Holocene optimum of the East Asian monsoon. Quaternary Science Reviews 19, 743–762.

Barber, D.C., Dyke, A., Hillaire-Marcel, C., Jennings, A.E., Andrews, J.T., Kerwin, M.W., Bilodeau, G., McNeely, R., Southon, J.,

Morehead, M.D., Gagnon, J.M., 1999. Forcing of the cold event of 8200 years ago by catastrophic drainage of Laurentide lakes. Nature 400, 344–348.

Barnett, T.P., Dumenil, L., Schlese, U., Roeckner, E., 1988. The effect of Eurasian snow cover on global climate. Science 239, 504–507.

Berger, A., Loutre, M.F., 1991. Insolation values for the climate of the last 10 million years. Quaternary Science Reviews 10, 297–317.

Bradley, R.S., 1999. Paleoclimatology. Reconstructing Climates of the Quaternary. Academic Press, New York, 613p.

Bray, H.E., Stokes, S., 2004. Temporal patterns of arid-humid transitions in the south-eastern Arabian Peninsula based on optical dating. Geomorphology 59, 271–280.

Burns, S.J., Matter, A., Frank, N., Mangini, A., 1998. Speleothem-based paleoclimate record from northern Oman. Geology 26, 499–502.

Burns, S.J., Fleitmann, D., Matter, A., Neff, U., Mangini, A., 2001. Speleothem evidence from Oman for continental pluvial events during interglacial periods. Geology 29, 623–626.

Burns, S.J., Fleitmann, D., Mudelsee, M., Neff, U., Matter, A., Mangini, A., 2002. A 780-year annually resolved record of Indian Ocean monsoon precipitation from a speleothem from south Oman. Journal of Geophysical Research-Atmospheres 107, art. no. 4434.

Burns, S.J., Fleitmann, D., Matter, A., Kramers, J., Al-Subbary, A.A., 2003. Indian Ocean climate and an absolute chronology over Dansgaard/Oeschger events 9 to 13. Science 301, 1365–1367.

Bush, A.B.G., in press. Temporal variability of the South Asian Monsoon through the Late Quaternary: results from AGCM and AOGCM simulations. Geological Society of India.

Camberlin, P., Okoola, R.E., 2003. The onset and cessation of the "long rains" in eastern Africa and their interannual variability. Theoretical and Applied Climatology, doi:10.1007/s00704-002-0721-5.

Chao, W.C., Chen, B., 2001. The origin of monsoons. Journal of the Atmospheric Sciences 58, 3497–3507.

Cheng, H., Edwards, R.L., Hoff, J., Gallup, C.D., Richards, D.A., Asmerom, Y., 2000. The half-lives of uranium-234 and thorium-230. Chemical Geology 169, 17–33.

Clark, I.D., Fritz, P., Quinn, O.P., Rippon, P.W., Nash, H., Bin Ghalib Al Said, B., 1987. Modern and fossil groundwater in an arid environment: a look at the hydrogeology of southern Oman. Use of stable isotopes in water resources development. IAEA Symposium 299, 167–187.

Clemens, S., Prell, W., Murray, D., Shimmield, G., Weedon, G., 1991. Forcing mechanisms of the Indian-Ocean Monsoon. Nature 353, 720–725.

Dansgaard, W., 1964. Stable isotopes in precipitation. Tellus 16, 436–468.

Dansgaard, W., Johnsen, S.J., Clausen, H.B., Dahl-Jensen, D., Gundestrup, N.S., Hammer, C.U., Hvidberg, C.S., Steffensen, J.P., Sveinbjörnsdottir, A.E., Jouzel, J., Bond, G., 1993. Evidence for general instability of past climate from a 250-ka ice-core record. Nature 364, 218–220.

deMenocal, P.E.A., 2000. Abrupt onset and termination of the African Humid Period: rapid climate responses to gradual insolation forcing. Quaternary Science Reviews 19, 347–361.

Denniston, R.F., Gonzalez, L.A., Asmerom, Y., Sharma, R.H., Reagan, M.K., 2000. Speleothem evidence for changes in Indian summer monsoon precipitation over the last similar to 2300 years. Quaternary Research 53, 196–202.

Dykoski, C.A., Edwards, R.L., Cheng, H., Yuan, D.X., Cai, Y.J., Zhang, M.L., Lin, Y.S., Qing, J.M., An, Z.S., Revenaugh, J., 2005. A high-resolution, absolute-dated Holocene and deglacial Asian monsoon record from Dongge Cave, China. Earth and Planetary Science Letters 233, 71–86.

Enzel, Y., Ely, L.L., Mishra, S., Ramesh, R., Amit, R., Lazar, B., Rajaguru, S.N., Baker, V.R., Sandler, A., 1999. High-resolution Holocene environmental changes in the Thar Desert, northwestern India. Science 284, 125–128.

Fleitmann, D., Burns, S.J., Mudelsee, M., Neff, U., Kramers, J., Mangini, A., Matter, A., 2003a. Holocene forcing of the Indian monsoon recorded in a stalagmite from Southern Oman. Science 300, 1737–1739.

Fleitmann, D., Burns, S.J., Neff, U., Mangini, A., Matter, A., 2003b. Changing moisture sources over the last 330,000 years in Northern Oman from fluid-inclusion evidence in speleothems. Quaternary Research 60, 223–232.

Fleitmann, D., Burns, S.J., Neff, U., Mudelsee, M., Mangini, A., Matter, A., 2004. Palaeoclimatic interpretation of high-resolution oxygen isotope profiles derived from annually laminated speleothems from Southern Oman. Quaternary Science Reviews 23, 935–945.

Fontes, J.C., Gasse, F., Gibert, E., 1996. Holocene environmental changes in Bangong Co Basin (Western Tibet). Part 1: chronology and stable isotopes of carbonates of a Holocene lacustrine core. Palaeogeography, Palaeoclimatology, Palaeoecology 120, 25–47.

Frank, N., Braum, M., Hambach, U., Mangini, A., Wagner, G., 2000. Warm period growth of Travertine during the Last Interglaciation in Southern Germany. Quaternary Research 54, 38–48.

Findlater, J., 1969. Interhemispheric transport of air in lower troposphere over Western Indian Ocean. Quarterly Journal of the Royal Meteorological Society 95, 362–380.

Gadgil, S., 2003. The Indian monsoon and its variability. Annual Reviews of Earth and Planetary Sciences 31, 429–467.

Gasse, F., Fontes, J.C., VanCampo, E., Wei, K., 1996. Holocene environmental changes in Bangong Co basin (western Tibet).4. Discussion and Conclusions: Palaeogeography Palaeoclimatology Palaeoecology 120, 79–92.

Gasse, F., 2000. Hydrological changes in the African tropics since the Last Glacial Maximum. Quaternary Science Reviews 19, 189–211.

Genty, D., Quinif, Y., 1996. Annually laminated sequences in the internal structure of some Belgian stalagmites-Importance for Paleoclimatology. Journal of Sedimentary Research 66, 275–288.

Gu, Z., Liu, J., Yuan, B., Liu, T., Liu, R., Liu, Y., Zhang, G., Yasukawa, K., 1993. The changes in monsoon influence in the Qinghai Tibet plateau during the past 12,000 years. Geochemical evidence from the lake Seling sediments. Chinese Science Bulletin 38, 61–64 (in Chinese).

Gupta, A.K., 2004. Origin of agriculture and domestication of plants and animals linked to early Holocene climate amelioration. Current Science 87, 54–59.

Gupta, A.K., Anderson, D.M., Overpeck, J.T., 2003. Abrupt changes in the Asian southwest monsoon during the Holocene and their links to the North Atlantic Ocean. Nature 421, 354–357.

Halpern, D., Woiceshyn, P.M., 2001. Somali Jet in the Arabian Sea, El Nino, and India rainfall. Journal of Climate 14, 434–441.

Haug, G.H., Hughen, K.A., Sigman, D.M., Peterson, L.C., Rohl, U., 2001. Southward migration of the intertropical convergence zone through the Holocene. Science 293, 1304–1308.

He, Y., Theakstone, W.H., Zhang, Z.L., Zhang, D.A., Yao, T.D., Chen, T., Shen, Y.P., Pang, H.X., 2004. Asynchronous Holocene climatic change across China. Quaternary Research 61, 52–63.

Hong, Y.T., Hong, B., Lin, Q.H., Zhu, Y.X., Shibata, Y., Hirota, M., Uchida, M., Leng, X.T., Jiang, H.B., Xu, H., Wang, H., Yi, L., 2003. Correlation between Indian Ocean summer monsoon and North Atlantic climate during the Holocene. Earth and Planetary Science Letters 211, 371–380.

Ivanochko, T.S., Ganeshram, R.S., Brummer, G.-J., Brummer, A., Ganssen, G., Jung, S.J.A., Moreton, S.G., Kroon, D., 2005. Variations in tropical convection as an amplifier of global climate change at the millennial scale. Earth and Planetary Science Letters 235, 302–314.

Johnsen, S.J., Dahl-Jensen, D., Gundestrup, N., Steffensen, J.P., Clausen, H.B., Miller, H., Masson-Delmotte, V., Sveinbjornsdottir, A.E., White, J., 2001. Oxygen isotope and palaeotemperature records from six Greenland ice-core stations: camp century, Dye-3, GRIP, GISP2, Renland and NorthGRIP. Journal of Quaternary Science 16, 299–307.

Johnson, K.R., Ingram, B.L., 2004. Spatial and temporal variability in the stable isotope systematics of modern precipitation in China: implications for paleoclimate reconstructions. Earth and Planetary Science Letters 220, 365–377.

Ju, J.H., Slingo, J., 1995. The Asian summer monsoon and ENSO. Quarterly Journal of the Royal Meteorological Society 121, 1133–1168.

Jung, S.J.A., Davies, G.R., Ganssen, G., Kroon, D., 2002. Decadal-centennial scale monsoon variations in the Arabian Sea during the Early Holocene. Geochemistry Geophysics Geosystems 3, art. no.-1060.

Jung, S.J.A., Davies, G.R., Ganssen, G.M., Kroon, D., 2004. Stepwise Holocene aridification in NE Africa deduced from dust-borne radiogenic isotope records. Earth and Planetary Science Letters 221, 27–37.

Leuschner, D.C., Sirocko, F., 2000. The low-latitude monsoon climate during Dansgaard–Oeschger cycles and Heinrich Events. Quaternary Science Reviews 19, 243–254.

Lézine, A.M., Saliége, J.F., Robert, C., Wertz, F., Inizan, M.L., 1998. Holocene lakes from Ramlat as-Sab'atayn (Yemen) illustrate the impact of monsoon activity in Southern Arabia. Quaternary Research 50, 290–299.

Lister, G.S., Kelts, K., Zao, C.K., Yu, J.Q., Niessen, F., 1991. Lake Qinghai, China—Closed-Basin Lake Levels and the Oxygen Isotope Record for Ostracoda since the Latest Pleistocene. Palaeogeography Palaeoclimatology Palaeoecology 84, 141–162.

Lũckge, A., Doose-Rolinski, H., Khan, A.A., Schulz, H., von Rad, U., 2001. Monsoonal variability in the northeastern Arabian Sea during the past 5000 years: geochemical evidence from laminated sediments. Palaeogeography Palaeoclimatology Palaeoecology 167, 273–286.

Maslin, M.A., Burns, S.J., 2000. Reconstruction of the Amazon Basin effective moisture availability over the past 14,000 years. Science 290, 2285–2287.

McClure, H.A., 1976. Radiocarbon chronology of late Quaternary lakes in the Arabiam Desert. Nature 263, 755–756.

Mies, B., Beyhl, F.E., 1996. The Vegetation Ecology of Soqotra. In: Dumont, H.J., (Ed.), Proceedings of the First International Symposium on Soqotra Island: Present and Future. United Nations Publications, New York, pp. 35–82.

Morrill, C., Overpeck, J.T., Cole, J.E., 2003. A synthesis of abrupt changes in the Asian summer monsoon since the last deglaciation. Holocene 13, 465–476.

Mudelsee, V., 2006. CLIM-X-DETECT: A Fortran 90 program for robust detection of extremes against a time-dependent background in climate records. Computer and Geosciences 32, 141–144.

Narayanan, M.S., Rao, B.M., 1981. Detection of Monsoon Inversion by Tiros-N Satellite. Nature 294, 546–548.

Neff, U., Burns, S.J., Mangini, A., Mudelsee, M., Fleitmann, D., Matter, A., 2001. Strong coherence between solar variability and the monsoon in Oman between 9 and 6 ka ago. Nature 411, 290–293.

Overpeck, J., Anderson, D., Trumbore, S., Prell, W., 1996. The southwest Indian Monsoon over the last 18000 years. Climate Dynamics 12, 213–225.

Parker, A.G., Eckersley, L., Smith, M.M., Goudie, A.S., Stokes, S., Ward, S., White, K., Hodson, M.J., 2004. Holocene vegetation dynamics in the northeastern Rub' al-Khali desert, Arabian Peninsula: a phytolith, pollen and carbon isotope study. Journal of Quaternary Science 19, 665–676.

Prasad, S., Kusumgar, S., Gupta, S.K., 1997. A mid to late Holocene record of palaeoclimatic changes from Nal Sarovar: a palaeodesert margin lake in western India. Journal of Quaternary Science 12, 153–159.

Prell, W.L., Kutzbach, J.E., 1987. Monsoon variability over the past 150,000 years. Journal of Geophysical Research-Atmospheres 92, 8411–8425.

Prell, W.L., Kutzbach, J.E., 1992. Sensitivity of the Indian Monsoon to forcing Parameters and implications for its evolution. Nature 360, 647–652.

Polyak, V.J., Asmerom, Y., 2001. Late Holocene climate and cultural changes in the southwestern United States. Science 294, 148–151.

Radies, D., Preusser, F., Matter, A., Mange, M., 2004. Eustatic and climatic controls on the development of the Wahiba Sand Sea, Sultanate of Oman. Sedimentology 51, 1359–1385.

Rozanski, K., Araguasaraguas, L., Gonfiantini, R., 1992. Relation between long-term trends of O-18 isotope composition of precipitation and climate. Science 258, 981–985.

Sarkar, A., Ramesh, R., Somayajulu, B.L.K., Agnihotri, R., Jull, A.J.T., Burr, G.S., 2000. High resolution Holocene monsoon record from the eastern Arabian Sea. Earth and Planetary Science Letters 177, 209–218.

Seltzer, G., Rodbell, D., Burns, S., 2000. Isotopic evidence for late Quaternary climatic change in tropical South America. Geology 28, 35–38.

Schulz, H., von Rad, U., Erlenkeuser, H., 1998. Correlation between Arabian Sea and Greenland climate oscillations of the past 110,000 years. Nature 393, 54–57.

Singh, G., Joshi, R.D., Chopra, S.K., Singh, A.B., 1974. Late Quaternary history of vegetation and climate of the Rajasthan Desert, India. Philosophical Transactions of the Royal Society of London 267, 467–501.

Sirocko, F., Sarnthein, M., Lange, H., Erlenkeuser, H., 1991. Atmospheric summer circulation and coastal upwelling in the Arabian Sea during the Holocene and the Last Glaciation. Quaternary Research 36, 72–93.

Sirocko, F., Sarnthein, M., Erlenkeuser, H., Lange, H., Arnold, M., Duplessy, J.C., 1993. Century-scale events in monsoonal climate over the past 24,000 years. Nature 364, 322–324.

Staubwasser, M., Sirocko, F., Grootes, P. M., Erlenkeuser, H., 2002. South Asian monsoon climate change and radiocarbon in the Arabian Sea during early and middle Holocene. Paleoceanography 17, doi:10.1029/2000PA000608.

Staubwasser, M., Sirocko, F., Grootes, P. M., Segl, M., 2003. Climate change at the 4.2 ka BP termination of the Indus valley civilization and Holocene south Asian monsoon variability. Geophysical Research Letters 30, doi:10.1029/2002GL016822.

Stuiver, M., Reimer, P.J., Braziunas, T.F., 1998. High-precision radiocarbon age calibration for terrestrial and marine samples. Radiocarbon 40, 1127–1151.

Teller, J.T., Leverington, D.W., 2004. Glacial Lake Agassiz: A 5000 yr history of change and its relationship to the delta O-18 record of Greenland. Geological Society of America Bulletin 116, 729–742.

Thompson, L.G., Yao, T., Mosley-Thompson, E., Davis, M.E., Henderson, K.A., Lin, P.-N., 2000. A high-resolution millennial record of the South Asian monsoon from Himalayan ice cores. Science 289, 1916–1919.

von Rad, U., Schaaf, M., Michels, K.H., Schulz, H., Berger, W.H., Sirocko, F., 1999. A 5000-yr record of climate change in varved sediments from the oxygen minimum zone off Pakistan, Northeastern Arabian Sea. Quaternary Research 51, 39–53.

Wang, Y.J., Cheng, H., Edwards, R.L., An, Z.S., Wu, J.Y., Shen, C.C., Dorale, J.A., 2001. A high-resolution absolute-dated Late Pleistocene monsoon record from Hulu Cave, China. Science 294, 2345–2348.

Wang, Y.J., Cheng, H., Edwards, R.L., He, Y.Q., Kong, X.G., An, Z.S., Wu, J.Y., Kelly, M.J., Dykoski, C.A., Li, X.D., 2005. The Holocene Asian monsoon: links to solar changes and North Atlantic climate. Science 308, 854–857.

Webster, P.J., Magana, V.O., Palmer, T.N., Shukla, J., Tomas, R.A., Yanai, M., Yasunari, T., 1998. Monsoons: processes, predictability, and the prospects for prediction. Journal of Geophysical Research-Oceans 103, 14451–14510.

Wei, K., Gasse, F., 1999. Oxygen isotopes in lacustrine carbonates of West China revisited: implications for post glacial changes in summer monsoon circulation. Quaternary Science Reviews 18, 1315–1334.

Weyhenmeyer, C.E., Burns, S.J., Waber, H.N., Aeschbach-Hertig, W., Kipfer, R., Loosli, H.H., Matter, A., 2000. Cool glacial temperatures and changes in moisture source recorded in Oman groundwaters. Science 287, 842–845.

Weyhenmeyer, C.E., Burns, S.J., Waber, H.N., Macumber, P.G., Matter, A., 2002. Isotope study of moisture sources, recharge areas, and groundwater flow paths within the eastern Batinah coastal plain, Sultanate of Oman. Water Resources Research 38, 1184.

Yadava, M.G., Ramesh, R., Pant, G.B., 2004. Past monsoon rainfall variations in peninsular India recorded in a 331-year-old speleothem. Holocene 14, 517–524.

Ye, H.C., Bao, Z.H., 2001. Lagged teleconnections between snow depth in northern Eurasia, rainfall in Southeast Asia and sea-surface temperatures over the tropical Pacific Ocean. International Journal of Climatology 21, 1607–1621.